

**UCLA**

**UCLA Electronic Theses and Dissertations**

**Title**

Computational Modeling of Ni-Based Catalysts for Selective Hydrogenation of Acetylene to Ethylene

**Permalink**

<https://escholarship.org/uc/item/74c1n036>

**Author**

Almisbaa, Zahra

**Publication Date**

2021

Peer reviewed|Thesis/dissertation

UNIVERSITY OF CALIFORNIA

Los Angeles

Computational Modeling of Ni-Based Catalysts for Selective Hydrogenation of Acetylene to  
Ethylene

A thesis submitted in partial satisfaction

of the requirements for the degree

Master of Science in Chemical Engineering

by

Zahra Nasser Almisbaa

2021

© Copyright by

Zahra Nasser Almisbaa

2021

## ABSTRACT OF THE THESIS

Computational Modeling of Ni-Based Catalysts for Selective Hydrogenation of Acetylene to  
Ethylene

by

Zahra Nasser Almisbaa

Master of Science in Chemical Engineering

University of California, Los Angeles, 2021

Professor Philippe Sautet, Chair

DFT-based modeling of  $\text{Ni}_2\text{In}_3$  (110) and  $\text{NiSi}_2$  (101) intermetallic surfaces was used to describe surface chemistry during acetylene hydrogenation and oligomerization reactions. The adsorption energies of partially and completely isolated Ni active sites were investigated in  $\text{Ni}_2\text{In}_3$  and  $\text{NiSi}_2$ , respectively. The activity and selectivity of the catalysts were benchmarked against monometallic Ni surface. Despite the weak adsorption of acetylene and ethylene on the  $\text{Ni}_2\text{In}_3$  (110), selectivity toward ethylene was not enhanced. Acetylene oligomerization was favorable on  $\text{Ni}_2\text{In}_3$  (110) and competed with acetylene hydrogenation.  $\text{NiSi}_2$  (101) exhibited strong acetylene adsorption and suppressed green oil formation. Hydrocarbon molecules on  $\text{NiSi}_2$  (101) were activated by Si and Ni atoms, while In atoms showed low activity toward hydrogen and hydrocarbon molecules.

The thesis of Zahra Nasser Almisbaa is approved.

Dante A. Simonetti

Carlos Gilber Morales Guio

Philippe Sautet, Committee Chair

University of California, Los Angeles

2021



# CONTENTS

INTRODUCTION .....	1
METHODS .....	9
2.1 Computational method .....	9
2.2 Bulk unit cells.....	10
Surface Modeling.....	12
3.1 Surface facets and surface energy .....	12
3.2 Surveying Adsorption Sites.....	17
3.3 Thermochemical Analysis.....	24
Acetylene Hydrogenation Reaction Profiles.....	27
Acetylene Oligomerization Reaction Profiles .....	36
Conclusion and Future Work.....	44
APPENDIX.....	47
7.1 Adsorption Sites and Reaction Energies of Intermediates .....	47
7.2 Hydrogen Adsorption Sites and Reaction Energies .....	48
7.3 Other Bulk Lattice Calculations .....	48
BIBLIOGRAPHY .....	50

## LIST OF FIGURES

Figure 1.1: In-Ni phase diagram from Okamoto et al. (26) .....	6
Figure 1.2: Ni-Si phase diagram from Okamoto et al. (27) .....	7
Figure 3.1: Top and side views of (a) Ni (111) (b) Ni <sub>2</sub> In <sub>3</sub> (110) with partially isolated Ni active sites and (c) NiSi <sub>2</sub> (101) with completely isolated Ni active sites.....	16
Figure 3.2: Most stable acetylene and ethylene configurations on Ni (111), Ni <sub>2</sub> In <sub>3</sub> (110) and NiSi <sub>2</sub> (101).....	20
Figure 3.3: Hydrogen adsorption sites on Ni <sub>2</sub> In <sub>3</sub> (110) surface before and after optimization. ...	22
Figure 3.4: Hydrogen adsorption sites on NiSi <sub>2</sub> (101) before and after optimization. ....	23
Figure 4.1: Acetylene hydrogenation reaction profile on Ni <sub>2</sub> In <sub>3</sub> (110) and monometallic Ni catalysts.....	29
Figure 4.2: Acetylene hydrogenation reaction profile on NiSi <sub>2</sub> (101) and monometallic Ni catalysts.....	30
Figure 4.3: Structures of transition states in acetylene hydrogenation pathway on Ni (111): (a) Hydrogenation of adsorbed acetylene to form vinyl. (b) Vinyl hydrogenation to form ethylene. (c) Ethylene hydrogenation to form C <sub>2</sub> H <sub>5</sub> . (d) Hydrogenation of C <sub>2</sub> H <sub>5</sub> to form ethane. IS: initial state, TS: transition state, FS: final state. ....	33
Figure 4.4: Structures of transition states in acetylene hydrogenation pathway on Ni <sub>2</sub> In <sub>3</sub> (110): (a) Hydrogenation of adsorbed acetylene to form vinyl. (b) Vinyl hydrogenation to form ethylene. (c) Ethylene hydrogenation to form C <sub>2</sub> H <sub>5</sub> . (d) Hydrogenation of C <sub>2</sub> H <sub>5</sub> to form ethane. IS: initial state, TS: transition state, FS: final state. ....	34
Figure 4.5: Structures of transition states in acetylene hydrogenation pathway on NiSi <sub>2</sub> (101): (a) Hydrogenation of adsorbed acetylene to form vinyl. (b) Vinyl hydrogenation to form ethylene. (c)	



Ethylene hydrogenation to form C <sub>2</sub> H <sub>5</sub> . (d) Hydrogenation of C <sub>2</sub> H <sub>5</sub> to form ethane. IS: initial state, TS: transition state, FS: final state. ....	35
Figure 5.1: Acetylene oligomerization reaction profile of Ni <sub>2</sub> In <sub>3</sub> and monometallic Ni catalysts. ....	39
Figure 5.2: Acetylene oligomerization reaction profile of NiSi <sub>2</sub> and monometallic Ni catalysts.	39
Figure 5.3: Structures of transition states for the acetylene oligomerization pathway on Ni (111): (a) C-C bond formation between absorbed acetylene and vinyl molecules. (b) Hydrogenation of absorbed C <sub>4</sub> H <sub>5</sub> to form butadiene. IS: initial state, TS: transition state, FS: final state.....	41
Figure 5.4: Structures of transition states for the acetylene oligomerization pathway on Ni <sub>2</sub> In <sub>3</sub> (110): (a) C-C bond formation between absorbed acetylene and vinyl molecules. (b) Hydrogenation of absorbed C <sub>4</sub> H <sub>5</sub> to form butadiene. IS: initial state, TS: transition state, FS: final state. ....	42
Figure 5.5: Structures of transition states for the acetylene oligomerization pathway on NiSi <sub>2</sub> (101): (a) C-C bond formation between absorbed acetylene and vinyl molecules. (b) Hydrogenation of absorbed C <sub>4</sub> H <sub>5</sub> to form butadiene. IS: initial state, TS: transition state, FS: final state. ....	43
Figure 7.1: Adsorption energy (eV) correlation with number of adsorbed H atoms. ....	48

## LIST OF TABLES

Table 2.1: Bulk unit cells of Ni, Ni <sub>2</sub> In <sub>3</sub> and NiSi <sub>2</sub> shown in top and side views.....	10
Table 2.2: Space group, crystal system and bulk unit cell energy (eV).....	11
Table 2.3: Bulk lattice parameters (Å) calculated using DFT-D3 and GGA-PBE and compared to experimental values. The two numbers in Ni <sub>2</sub> In <sub>3</sub> lattice (hcp) correspond to a and c, respectively. .....	11
Table 3.1: Surface energy (J/m <sup>2</sup> ) and coverage for low-index facets of the Ni <sub>2</sub> In <sub>3</sub> slab. Elements are colored: Ni (green) and In (brown). .....	12
Table 3.2: Surface energy (J/m <sup>2</sup> ) and coverage for low-index facets of the NiSi <sub>2</sub> slab. Elements are colored: Ni (green) and Si (beige).....	14
Table 3.3: Surface energy (J/m <sup>2</sup> ) of varied Si and Ni coverage for the (100) facet of NiSi <sub>2</sub> slab.	14
Table 3.4: Surface energy (J/m <sup>2</sup> ) of the most stable facets of Ni <sub>2</sub> In <sub>3</sub> and NiSi <sub>2</sub> at different thickness.....	15
Table 3.5: DFT-D3 calculated values of adsorption energies (eV) of acetylene, ethylene and H atom on Ni(111) compared to literature values (22)(42). (H atom value reference is ½ H <sub>2</sub> ) .....	17
Table 3.6: Adsorption energy of acetylene, ethylene, and H atom over Ni <sub>2</sub> In <sub>3</sub> (110) surface. ....	18
Table 3.7: Adsorption energy of acetylene, ethylene, and H atom over NiSi <sub>2</sub> (101) surface. ....	19
Table 3.8: Thermochemical analysis for free gaseous molecules in the hydrogenation reaction calculated using GGA-PBE and DFT-D3 methods. ....	25
Table 3.9: Enthalpy ΔH of ethylene and ethane formation calculated using GGA-PBE and DFT-D3 and compared to experimental literature values (2).....	26
Table 4.1: Acetylene adsorption energy and hydrogenation barrier (eV) on Ni (111), Ni <sub>2</sub> In <sub>3</sub> (110), and NiSi <sub>2</sub> (101).....	30

Table 4.2: Ethylene desorption barrier (eV), ethylene hydrogenation barrier (acetylene over-hydrogenation barrier) (eV) on Ni (111), Ni <sub>2</sub> In <sub>3</sub> (110), and NiSi <sub>2</sub> (101).....	31
Table 4.3: Ethane desorption barrier (eV) on Ni (111), Ni <sub>2</sub> In <sub>3</sub> (110), and NiSi <sub>2</sub> (101).....	31
Table 4.4: Distance (Å) between bonding C and H atoms from the initial state (IS) to the transition state (TS) on Ni (111), Ni <sub>2</sub> In <sub>3</sub> (110), and NiSi <sub>2</sub> (101). ....	31
Table 5.1: Comparison between the energy barrier (eV) of C-C coupling of acetylene and vinyl and the acetylene adsorption energy (eV) on Ni (111), Ni <sub>2</sub> In <sub>3</sub> (110), and NiSi <sub>2</sub> (101). ....	40
Table 5.2: Butadiene desorption energy barrier (eV) calculated based on butadiene molecule desorption energy -4.42 (eV) on Ni (111), Ni <sub>2</sub> In <sub>3</sub> (110), and NiSi <sub>2</sub> (101).....	40
Table 5.3: Initial state (IS) and transition state (TS) distance (Å) between two C bonding to form C <sub>4</sub> H <sub>5</sub> , and between attacking H and C atom in subsequent hydrogenation to form C <sub>4</sub> H <sub>6</sub> . ....	40
Table 7.1: Adsorption sites of gaseous molecules over Ni <sub>2</sub> In <sub>3</sub> (110) surface.....	47
Table 7.2: Adsorption sites of gaseous molecules over NiSi <sub>2</sub> (101) surface. ....	47
Table 7.3: Space group and bulk unit cell energy (eV) of Ni-based IMC systems. ....	48
Table 7.4: Bulk lattice parameters calculated using DFT-D3 and compared to experimental values. The two numbers in NiZn and Ni <sub>3</sub> Sn <sub>4</sub> lattice correspond to a and c, respectively.....	49

## PREFACE

This work received support from UCLA Institute of Digital Research and Education (IDRE) for computational resources on the UCLA Hoffman2 cluster.

This work used the Extreme Science and Engineering Discovery Environment (XSEDE) Expanse and Bridges-2 clusters at San Diego Supercomputer Center through allocation TG-CHE170060. XSEDE is supported by National Science Foundation Grant number ACI-1548562.

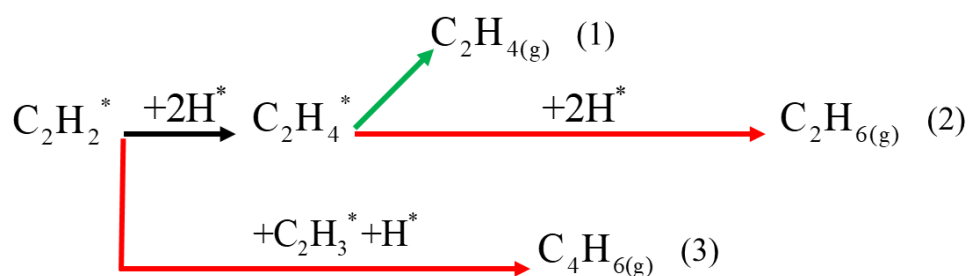
This work used the resources of the Supercomputing Laboratory at King Abdullah University of Science & Technology (KAUST) in Thuwal, Saudi Arabia.

The author gratefully acknowledged the financial sponsorship from Saudi Aramco.

# CHAPTER 1

## INTRODUCTION

Naphtha steam cracking is the primary source of ethylene production. Ethylene streams that come from steam crackers are the building blocks for polyethylene products and other key polymers. Acetylene is present in ethylene streams at levels of 1% and must be removed to an acceptable level of less than 5 ppm before the polymerization process (1)(2)(3). To purify streams from ppm levels of acetylene, highly active catalysts were developed to selectively hydrogenate acetylene to ethylene.



Scheme 1.1: Three possible products during acetylene hydrogenation. (1) acetylene semi-hydrogenation ends by desorbing ethylene. (2) acetylene over-hydrogenation ends by forming ethane. (3) acetylene oligomerization ends by forming 1,3-butadiene. Asterisk (\*) indicates adsorbed molecules and atoms.

Selectivity presents a critical measure in the hydrogenation reaction due to the detrimental impact of acetylene impurities on the life span of the catalyst, and the quality of the polymeric products (4)(5)(2). Scheme 1.1 shows the selective reaction producing ethylene (1) and the other unselective reactions producing ethane (2) and 1,3-butadiene (3). Selectivity is impacted by the further hydrogenation of ethylene to ethane, and the oligomerization of acetylene producing heavy C4 species known as “green oil”. These oligomeric species, composed mainly of 1,3-butadiene, (6)

(2) poison the active sites of the catalyst causing irreversible deactivation (5). They also obstruct the diffusion of acetylene on the reaction surface, and can rapidly consume hydrogen supply in undesired side reactions (2). The deteriorating effects of these oligomers during the catalytic process intensify the need to find innovative selective solutions.

The concept of active site isolation was first introduced in 1976 by Verbeek & Sachtler (7). Isolation of active sites addressed the “geometric effect” that favored the weak pi bonding, rather than di-sigma bonding of acetylene and ethylene. Selectivity in hydrogenation reactions was attributed to weak adsorption energies. For acetylene, weak adsorption was associated with less oligomerization (6). For ethylene, weak adsorption meant improved desorption from the catalyst surface, and enhanced selectivity (8). Extended active sites were responsible for the strong adsorption of acetylene molecules which subsequently catalyzed C-C coupling and formed green oil (1)(5)(6). Isolation of active sites also addressed the “electronic effect”, in which promoters modified the electronic structures of the metals (9)(4)(10)(2)(11). Both the “geometric effect”, and “electronic effect” can be controlled and tuned toward improving the selectivity of catalysts.

Palladium and Platinum based catalysts have been used for decades for hydrogenation reactions (1)(12). The promotional effect of In was studied experimentally and theoretically by Cao et al (13). The intermetallic Pd-In catalyst showed remarkable activity and selectivity increase in acetylene hydrogenation in comparison to monometallic Pd catalyst. The effect of weak surface adsorption also suppressed the formation of palladium hydrides which were precursors for producing ethane. It was found that ethylene selectivity was directly correlated with increasing In content on the surface. Si-promoted Pd catalysts were also studied for acetylene hydrogenation. The addition of Si decreased the presence of long-chain hydrocarbons, enhanced ethylene desorption, and reduced the risk of catalyst deactivation (14)(15). The promotional effect of Si was

mainly for increasing the selectivity, as the activity was comparable to monometallic Pd catalyst (15). Despite the improvements of Pd-based catalysts, the cost of Pd motivates the need to find economical noble metal-free alternatives.

Ni-based catalysts are promising candidates for the hydrogenation of alkynes, particularly the intermetallic compounds (IMC) (6)(4). An intermetallic is defined as a phase of a binary system where atoms are in an ordered arrangement. Recently, IMC have attracted interest due to their versatility (16)(17)(11). The advantages of IMC, also known as “ordered alloys”, in comparison to disordered alloys were pronounced by studying the “order effect” of binary systems that existed in ordered and disordered phases (8)(18). For example, the catalytic performance of Pd-Cu catalyst was evaluated in the ordered and disordered phase. Increased selectivity was obtained when Pd and Cu atoms were in ordered arrangement (19). Unlike disordered alloys, IMC offer more control over the ensemble of active sites, improved surface dispersion, and less risk of surface segregation (9)(11)(18). Surface segregation is a major drawback that exists especially in the high industrially utilized Pd-Ag alloys, where Pd islands create an ideal environment for acetylene oligomerization (20). In general, ordered alloys are known to exhibit high thermodynamic stability, making them suitable as model catalysts.

Experimentally, the nature of IMC materials presents a challenge in terms of synthesis. In previous reports, synthesized catalysts suffered from metal oxides impurities that were observed in the XRD analysis of these catalysts as well as the co-presence of other phases (4)(21). For example, the promotional effect of In in Ni-In IMC was investigated experimentally with various Ni/In ratios. However, the XRD analysis showed the presence of mixed phases in the catalyst material, and characterization did not confirm the well-defined IMC structure (4). The challenge of producing pure phase compositions is due to the lack of reported synthesis procedures for intermetallic

materials. These reasons may explain some inconsistencies that could be observed between experimental and theoretical studies (10).

In addition to experimental challenges, computational modeling of IMC requires significantly more calculations to explore all the possible adsorption sites in comparison to single metal surfaces. Computational modeling is based on the density functional theory (DFT), and plays a crucial role in exploring the morphology of the active sites, and understanding adsorbates interaction on surfaces (18). The magnitude of the required calculations varies with the symmetry of the bimetallic system. In the intermetallic phase, large site ensembles are more spread, thus, varying the possible adsorption sites that should be surveyed on the surface.

Developments in computing power made investigating IMC more accessible than before. Several advances have been reported in this field. A recent DFT study of Ni-Ga IMC reported high selectivity and stability in comparison to monometallic Ni catalyst. It was found that the complete isolation of Ni atoms facilitated pi adsorption, enhanced ethylene desorption, as well as decreased coke formation (22). A theoretical study done by Rao et al. investigated selective hydrogenation on different geometric structures of Ni-Sn IMC found that the surfaces with complete isolation of Ni atoms had a low desorption barrier for ethylene (23). Another DFT study by Song et al. had investigated Ni + B-group IMC (NiB, NiAl, NiGa, NiIn, and NiTi) of 1:1 bulk composition. It was found that bulk bonding, hydrogenation thermodynamics, and kinetics had a different nature in the studied IMC than in monometallic Ni. A wide computational screening of Ni IMC was reported by Studt et al. (24) in which NiZn was identified as a selective catalyst based on the low levels of ethane production. Later on, a study done by Spanjers et al. proved that ethane levels were not an accurate descriptor for ethylene selectivity because they neglected the contribution of acetylene oligomerization (6). Moreover, the catalytic evaluation of Ni-Zn IMC showed that achieving high



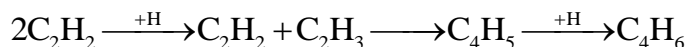
ethylene selectivity came at the expense of the turn-over frequency of the catalyst (6). The studies by Studt and Spanjers are an example of the lack of consensus in the literature regarding the surface chemistry of IMC for selective acetylene hydrogenation. However, the origin of selectivity in hydrogenation catalysts is still not fully understood.

The reaction mechanism of acetylene hydrogenation was investigated by Rao et al. and found that the ethylene pathway, shown in Scheme 1.2, is favored by Ni-based catalysts, and had lower effective barriers compared to the ethylidene intermediate pathway. Ethylidene is less likely to form when active sites are isolated (11). For the oligomerization pathway, shown in Scheme 1.2, C-C bond coupling between the adsorbed vinyl and acetylene molecules was found to be the most likely oligomerizing precursor (5)(6).

Acetylene hydrogenation pathway (ethylene pathway) (11):



Acetylene oligomerization pathway (6):



Scheme 1.2: Acetylene hydrogenation and oligomerization pathways.

In this work, two intermetallic formulations  $\text{Ni}_2\text{In}_3$  and  $\text{NiSi}_2$  were studied in the hydrogenation and oligomerization reaction pathways. In general, both Ni-Si and Ni-In IMC have been used for various hydrogenation reactions specifically in the hydrogenation of carbonyl compounds to their corresponding alcohols (21) (25).  $\text{Ni}_2\text{In}_3$  and  $\text{NiSi}_2$  exist in the intermetallic phase as shown in their phase diagrams in Figure 1.1 and Figure 1.2. Formulations with low content of Ni atoms were selected so that active site isolation could be applied. The selected formulations also had a

reasonable bulk unit cell size, and available synthesis recipes in the literature. Overall, the application of the selected IMC  $\text{NiSi}_2$  and  $\text{Ni}_2\text{In}_3$  formulations in the semi-hydrogenation of acetylene is not fully studied in the literature, despite their proven potential in other hydrogenation reactions.

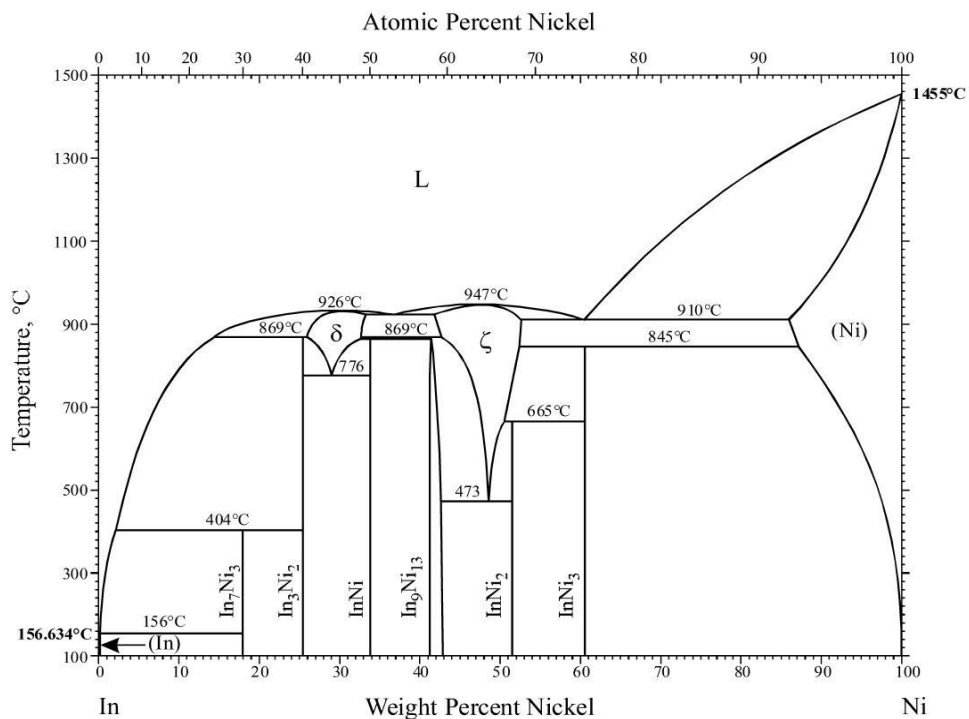


Figure 1.1: In-Ni phase diagram from Okamoto et al. (26)

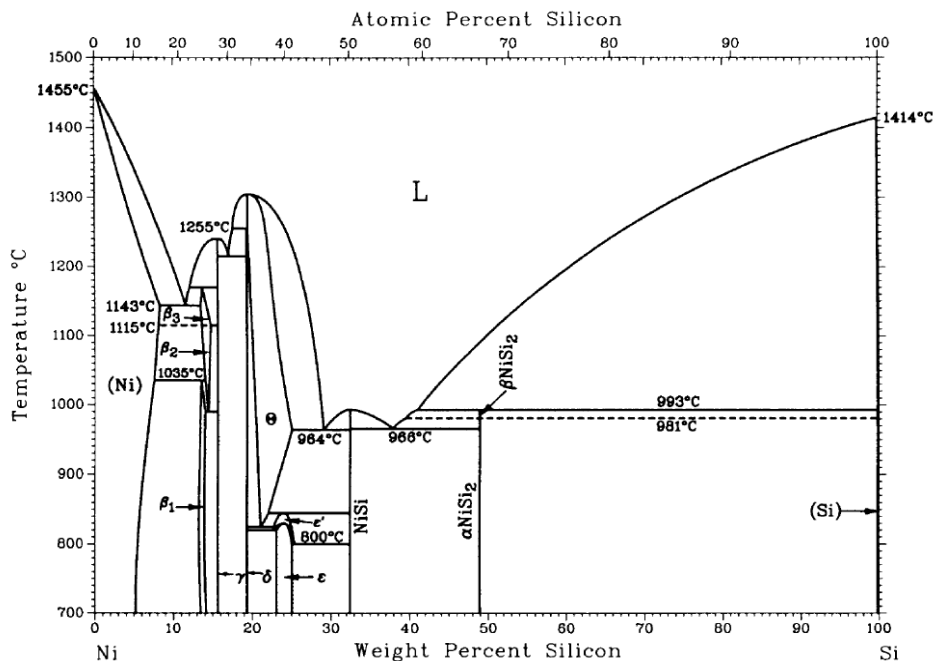


Figure 1.2: Ni-Si phase diagram from Okamoto et al. (27)

While the formation of green oil was extensively studied on Pd surfaces (5), no particular attention has been paid to the formation of green oil on Ni catalysts. Modifying the activity and the selectivity of Ni-based surfaces through the addition of promoters is still not fully explored. In this work, DFT is used to study acetylene hydrogenation over Ni, NiSi<sub>2</sub>, and Ni<sub>2</sub>In<sub>3</sub> surfaces, and develop insights about the reaction at an atomistic level. Monometallic Ni was included in the study to show the promotional effect of In and Si. It is proposed that the high coverage of the modifier In and Si with respect to the reactive transition metal Ni, offers an interesting case to study acetylene oligomerization in completely or partially isolated active site environments.

The thesis is organized as follows. Chapter 1 briefly explains the chemistry and reaction pathways, selectivity and the impact of acetylene oligomerization, motivations to search for noble metal-free alternatives, recent advances in hydrogenation catalysts, experimental and theoretical challenges of studying IMC. Chapter 2 presents the employed DFT method and IMC bulk units. Chapter 3

discusses surface facets and surface energy calculations, exploring the possible adsorption sites, and thermochemical analysis of the gaseous molecules. Chapter 4 discusses acetylene hydrogenation reaction profiles. Chapter 5 discusses acetylene oligomerization reaction profiles. Chapter 6 gives a summary of the findings and the path forward.

## CHAPTER 2

### METHODS

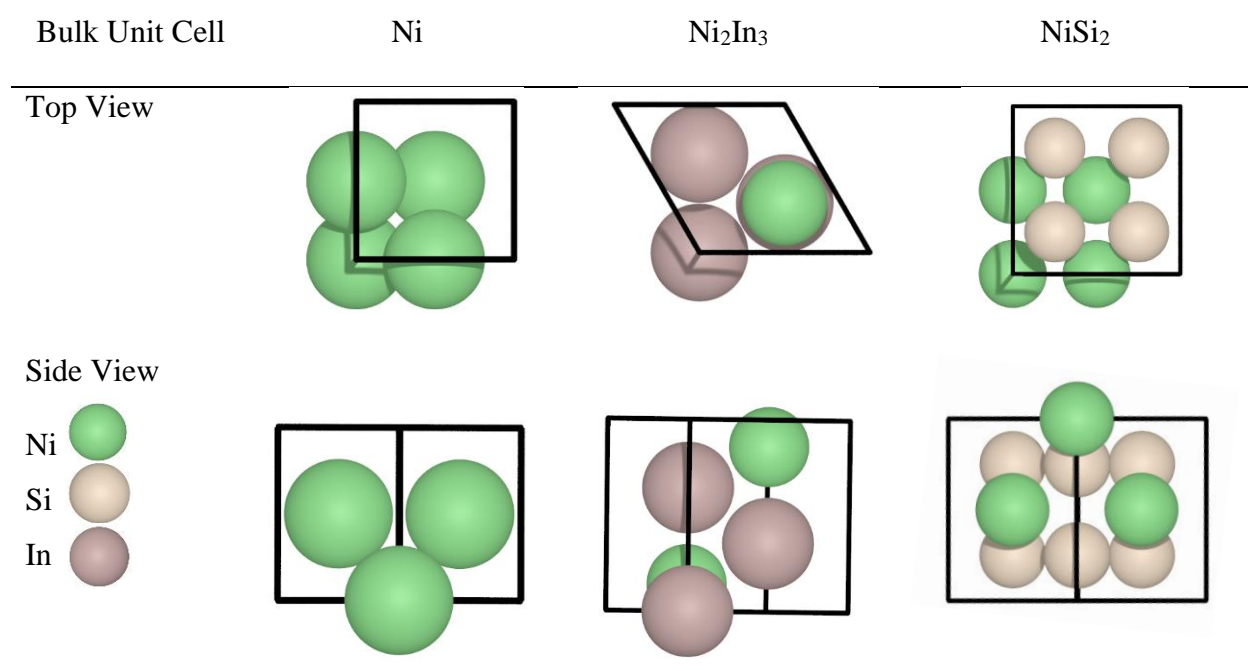
#### 2.1 Computational method

All DFT calculations were performed using the Vienna Ab-initio Simulation Package (VASP) (28) (29). The interaction between ionic core and valence electrons was described by the projector-augmented wave (PAW) potentials(30) (31). The valence one electron functions are developed on a basis set of planes waves with an energy cutoff of 400 eV. Exchange-correlation functional in the framework of the generalized gradient approximation (GGA-PBE) (32)was employed to calculate the electronic structure. Dispersion interactions were included using DFT-D3 method of Grimme (33) (34). Sampling the Brillouin zone was performed by  $3\times 3\times 1$  Monkhorst-Pack(35) k-point mesh for NiSi<sub>2</sub> surfaces,  $3\times 3\times 1$  and  $5\times 5\times 1$  Gamma-centered k-point mesh for Ni<sub>2</sub>In<sub>3</sub> and Ni surfaces, respectively. Force convergence threshold was set to 0.03 eV/Å and spin polarization was considered. Surfaces were modeled by p(2×2) supercells and four-atomic-layer slabs for monometallic Ni surface and Ni<sub>2</sub>In<sub>3</sub>. The slab for NiSi<sub>2</sub> was constructed with two-atomic-layer slabs due to the larger size of the bulk unit cell. Each slab was separated by a vacuum of 15 Å to eliminate the interaction between them. The two topmost layers and adsorbates were relaxed, and the rest of the layers were fixed except when calculating surface energies. Transition states were calculated using the climbing image-nudged elastic band (CI-NEB) method with 8 images (36). CI-NEB calculations were subsequently converged by Quasi-Newton method (IBRION=1) or the dimer method by Henkelman et al (37). Vibrational frequency calculations were used to verify transition states, resulting in one imaginary frequency along the reaction coordinate.

## 2.2 Bulk unit cells

IMC formulations of  $\text{Ni}_2\text{In}_3$  and  $\text{NiSi}_2$  were selected from their corresponding phase diagrams in Figure 1.1 and Figure 1.2. Overall, small unit cells were used because they are sufficient and to save computational costs, Ni unit cell was composed of 4 atoms,  $\text{Ni}_2\text{In}_3$  was 5 atoms and  $\text{NiSi}_2$  unit cell was 12 atoms. Initial bulk structures were obtained from the Materials Project (38). Unit Cells are shown in Table 2.1.

Table 2.1: Bulk unit cells of Ni,  $\text{Ni}_2\text{In}_3$  and  $\text{NiSi}_2$  shown in top and side views.



DFT-D3 was used for the rest of the calculations in this work because van der Waals interactions are an important component of the chemical bonds between the gaseous adsorbates and the surfaces in this reaction.

Details about crystal structures were obtained from the Materials Project (38) and bulk unit cell energies were optimized using DFT-D3 as presented in Table 2.2. Optimized bulk energies were later used to calculate surface energies.

Table 2.2: Space group, crystal system and bulk unit cell energy (eV).

Unit Cell	Number of Ni atoms	Number of other atoms	Space Group	Crystal System	Bulk Energy eV
Ni	4	0	Fm-3m	cubic	-23.60
NiSi <sub>2</sub>	4	8	Fm-3m	cubic	-73.13
Ni <sub>2</sub> In <sub>3</sub>	2	3	P-3m1	trigonal	-20.94

Lattice parameters of the bulk unit cells were calculated using DFT-D3 and GGA-PBE and compared with the experimental values as listed in Table 2.3. Values obtained using DFT-D3 were smaller than those obtained using GGA-PBE due to the inclusion of London-dispersion correction (39) as explained in equation (2.1).

$$E_{DFT-D3} = E_{Kohn-Sham} + E_{London-dispersion} \quad (2.1)$$

Table 2.3: Bulk lattice parameters (Å) calculated using DFT-D3 and GGA-PBE and compared to experimental values. The two numbers in Ni<sub>2</sub>In<sub>3</sub> lattice (hcp) correspond to a and c, respectively.

	DFT-D3	GGA-PBE	Experimental	Ref.	DFT-D3 Error%	GGA-PBE Error%
Ni	3.47	3.50	3.52	(6)	1.53	0.68
NiSi <sub>2</sub>	5.39	5.43	5.41	(40)	0.39	0.35
Ni <sub>2</sub> In <sub>3</sub> a	4.40	4.44	4.39	(41)	0.25	1.25
Ni <sub>2</sub> In <sub>3</sub> c	5.27	5.32	5.30		0.43	0.43

## CHAPTER 3

### Surface Modeling

#### 3.1 Surface facets and surface energy

The surface facet with the lowest energy corresponds to the most exposed surface. Surface energy  $\gamma$  is calculated using equation (3.1).

$$\gamma = \frac{(E_{slab} - NE_{bulk})}{2A} \quad (3.1)$$

Where  $E_{slab}$  is the total energy of the slab,  $N$  is the number of equivalent bulk unit cells for the slab and  $E_{bulk}$  is the energy of a single bulk unit cell.  $A$  is the area of the slab multiplied by a factor of 2 to account for top and bottom surface area. This equation assumes that top and bottom surfaces are equivalent.

Surface energy was calculated for five facets of  $Ni_2In_3$  slab and two facets of  $NiSi_2$  slab as shown in Table 3.1 and Table 3.2, respectively. Due to the symmetric nature of the  $NiSi_2$  slab, only two facets were investigated, and the rest of the facets were equivalent.  $\gamma$  values of the (100) facet were obtained with varied Si and Ni coverages as presented in Table 3.3. For the monometallic Ni surface, the (111) facet was selected because it was extensively studied in the literature, particularly in the acetylene hydrogenation reactions (6)(10)(11)(22).

Table 3.1: Surface energy ( $J/m^2$ ) and coverage for low-index facets of the  $Ni_2In_3$  slab. Elements are colored: Ni (green) and In (brown).



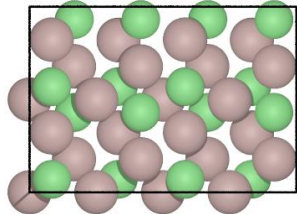
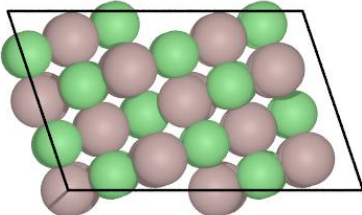
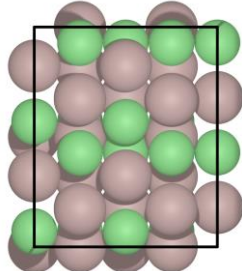
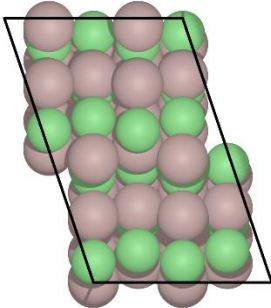
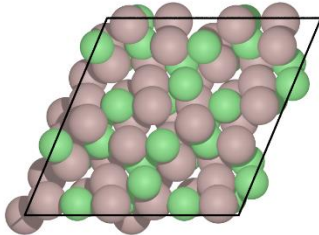
Surface Facet	Top View	Surface Energy J/m <sup>2</sup>
(110)		1.23
(101)		1.63
(100)		1.53
(011)		1.59
(111)		1.50

Table 3.2: Surface energy ( $\text{J/m}^2$ ) and coverage for low-index facets of the  $\text{NiSi}_2$  slab. Elements are colored: Ni (green) and Si (beige).

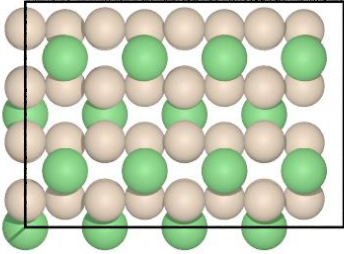
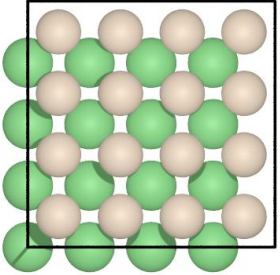
Surface Facet	Top View	Surface Energy $\text{J/m}^2$
(101)		1.53
(100)		1.94

Table 3.3: Surface energy ( $\text{J/m}^2$ ) of varied Si and Ni coverage for the (100) facet of  $\text{NiSi}_2$  slab.

Surface Facet	(100)	
Surface Energy $\text{J/m}^2$	2.39	1.75
Surface Coverage	half Si coverage	half Ni coverage

The effect of different slab thickness was studied by calculating the energy of 4 and 6 layers of  $\text{Ni}_2\text{In}_3$  (110), and 2 and 4 layers of  $\text{NiSi}_2$  (101). Values in Table 3.4 show proximity between the surface energies of different thicknesses. Lower number of layers was investigated in the case of

NiSi<sub>2</sub> (101) due to the large size of the unit cell. Reaction profiles were later calculated using 4 layers of the Ni<sub>2</sub>In<sub>3</sub> (110) and two layers of NiSi<sub>2</sub> (101).

Table 3.4: Surface energy (J/m<sup>2</sup>) of the most stable facets of Ni<sub>2</sub>In<sub>3</sub> and NiSi<sub>2</sub> at different thickness.

	Ni <sub>2</sub> In <sub>3</sub> (110)	NiSi <sub>2</sub> (101)
Thickness	4 layers	2 layers
Surface Energy J/m <sup>2</sup>	1.23	1.52
Thickness	6 layers	4 layers
Surface Energy J/m <sup>2</sup>	1.24	1.53

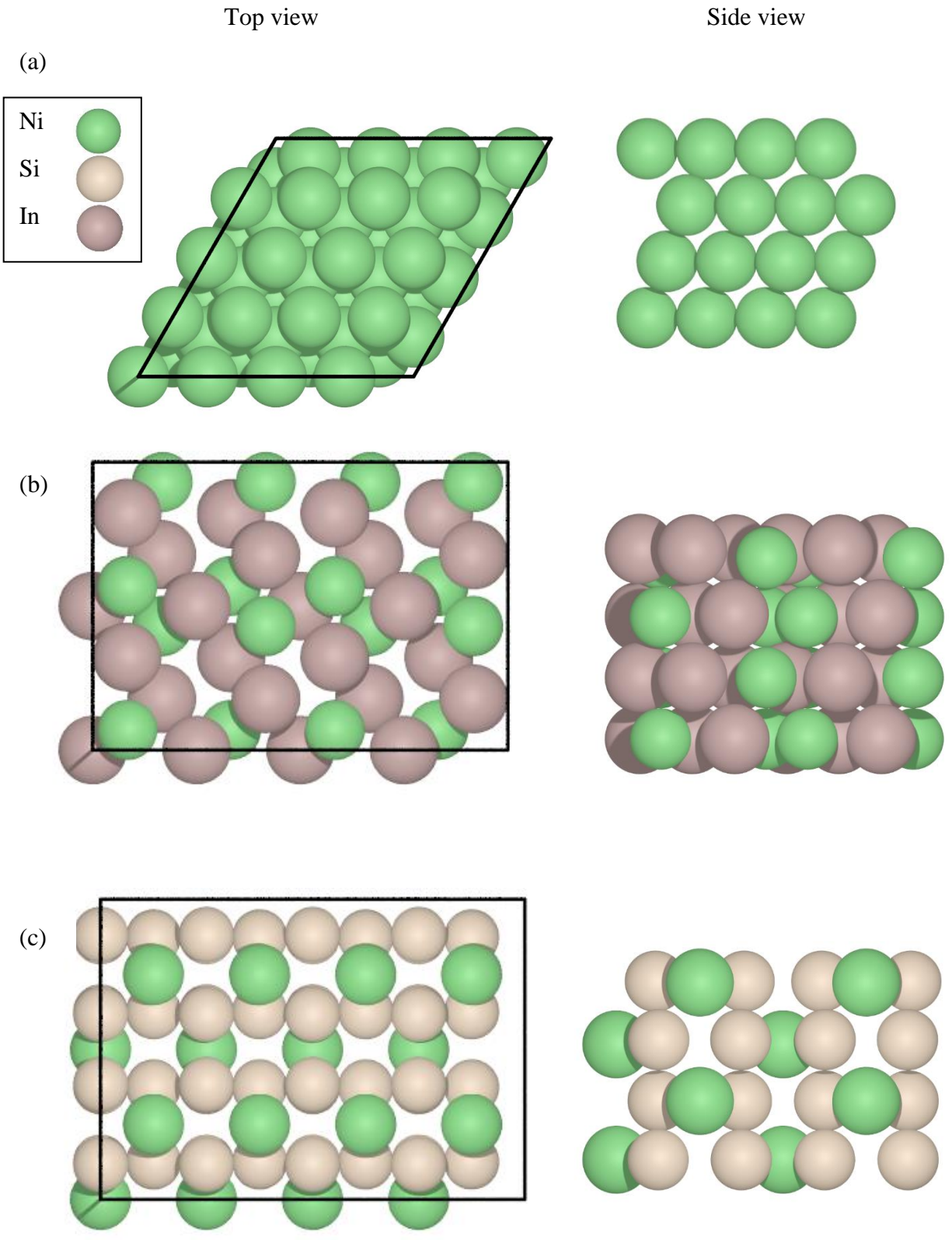


Figure 3.1: Top and side views of (a) Ni (111) (b)  $\text{Ni}_2\text{In}_3$  (110) with partially isolated Ni active sites and (c)  $\text{NiSi}_2$  (101) with completely isolated Ni active sites.

### 3.2 Surveying Adsorption Sites

The adsorption energy of the gaseous molecules was calculated following equation (3.2).

$$E_{adsorption} = E_{adsorbate/surface} - E_{surface} - E_{adsorbate} \quad (3.2)$$

Where  $E_{adsorption}$  is the adsorption energy,  $E_{adsorbate/surface}$  is the total energy of the gaseous molecule adsorbed on the surface of the slab,  $E_{surface}$  is the energy of the clean surface and  $E_{adsorbate}$  is the energy of the gaseous molecule. Adsorption energies of acetylene and ethylene over monometallic Ni surface were comparable to the values in the literature as presented in Table 3.5.

Table 3.5: DFT-D3 calculated values of adsorption energies (eV) of acetylene, ethylene and H atom on Ni(111) compared to literature values (22)(42). (H atom value reference is  $\frac{1}{2}$  H<sub>2</sub>)

Adsorption Energy eV	Calculated	Literature
Acetylene	-2.97	-2.98
Ethylene	-1.26	-1.28
H atom	-0.66	-0.64

Table 3.6 presents the values of adsorption energy of acetylene, ethylene, and H atom over the possible adsorption sites of Ni<sub>2</sub>In<sub>3</sub> (110) surface. The sites listed in Table 3.6 are the initial adsorption sites. Adsorbates may move to more stable sites upon optimization as shown in Figure 3.2 and Figure 3.3. Weak adsorption of acetylene and ethylene was evident over “In Top” and “Hollow of Ni and 2In” adsorption sites. Generally, weak adsorption energies were obtained over the surface including at the sites where Ni atoms were dominating. Hydrogen atoms were initially placed in the adsorption sites listed in Table 3.6. However, they could move to more stable sites upon geometric optimization as presented in Figure 3.3. H atoms were most stable at “Ni-Ni

Bridge” and “Hollow of In and 2Ni”. Acetylene and ethylene were also most stable over “Ni-Ni Bridge” and “Hollow of In and 2Ni”. The evaluation of the possible adsorption sites revealed that In atoms were less active than Ni atoms. The overall weak adsorption energies and low activity of In atoms came in agreement with the previous computational and experimental findings (4)(10).

Table 3.6: Adsorption energy of acetylene, ethylene, and H atom over Ni<sub>2</sub>In<sub>3</sub> (110) surface.

Adsorption Site/ Adsorbed Molecule	Ni Top	Ni-Ni Bridge	Ni-In Bridge	Hollow of In and 2Ni	Hollow of Ni and 2In	In Top
C <sub>2</sub> H <sub>2</sub>	-0.77	-1.24	-1.43	-1.43	-0.25	-0.24
C <sub>2</sub> H <sub>4</sub>	-0.68	-0.53	-0.68	-0.68	-0.22	-0.28
H	-0.21	-0.39	-0.21	-0.39	-0.21	-0.22

Table 3.7 presents the values of adsorption energy of acetylene, ethylene, and H atom over the possible adsorption sites of NiSi<sub>2</sub> (101) surface. Sites listed in Table 3.7 are the initial adsorption sites. Adsorbates may move to more stable sites upon optimization as shown in Figure 3.2 and Figure 3.4. The case of NiSi<sub>2</sub> (101) varied from Ni<sub>2</sub>In<sub>3</sub> (110). The most stable site for acetylene and ethylene adsorption was the “Si-Si bridge” site, demonstrating close values to the adsorption energies on monometallic Ni surface, presented in Table 3.5. Weak adsorption at “Ni Top” site was observed, where Ni atoms were completely isolated. Figure 3.4 shows hydrogen adsorption sites before and after geometric optimization. There was minimal movement of the H atom upon optimization. This indicates that H atom did not favor Ni sites over Si sites as was the case in Ni<sub>2</sub>In<sub>3</sub> (110). Moreover, positive H atom adsorption energy was obtained over all the adsorption sites on this surface including “Ni Top”, suggesting different activity towards H atom than acetylene and ethylene.

Table 3.7: Adsorption energy of acetylene, ethylene, and H atom over NiSi<sub>2</sub> (101) surface.

Adsorption Site/ Adsorbed Molecule	Ni Top	Ni-Si Bridge	Si-Si Bridge	Si Top
C <sub>2</sub> H <sub>2</sub>	-0.74	-1.14	-2.35	-0.17
C <sub>2</sub> H <sub>4</sub>	-0.75	-0.32	-1.41	-0.31
H	0.12	0.02	0.14	0.13

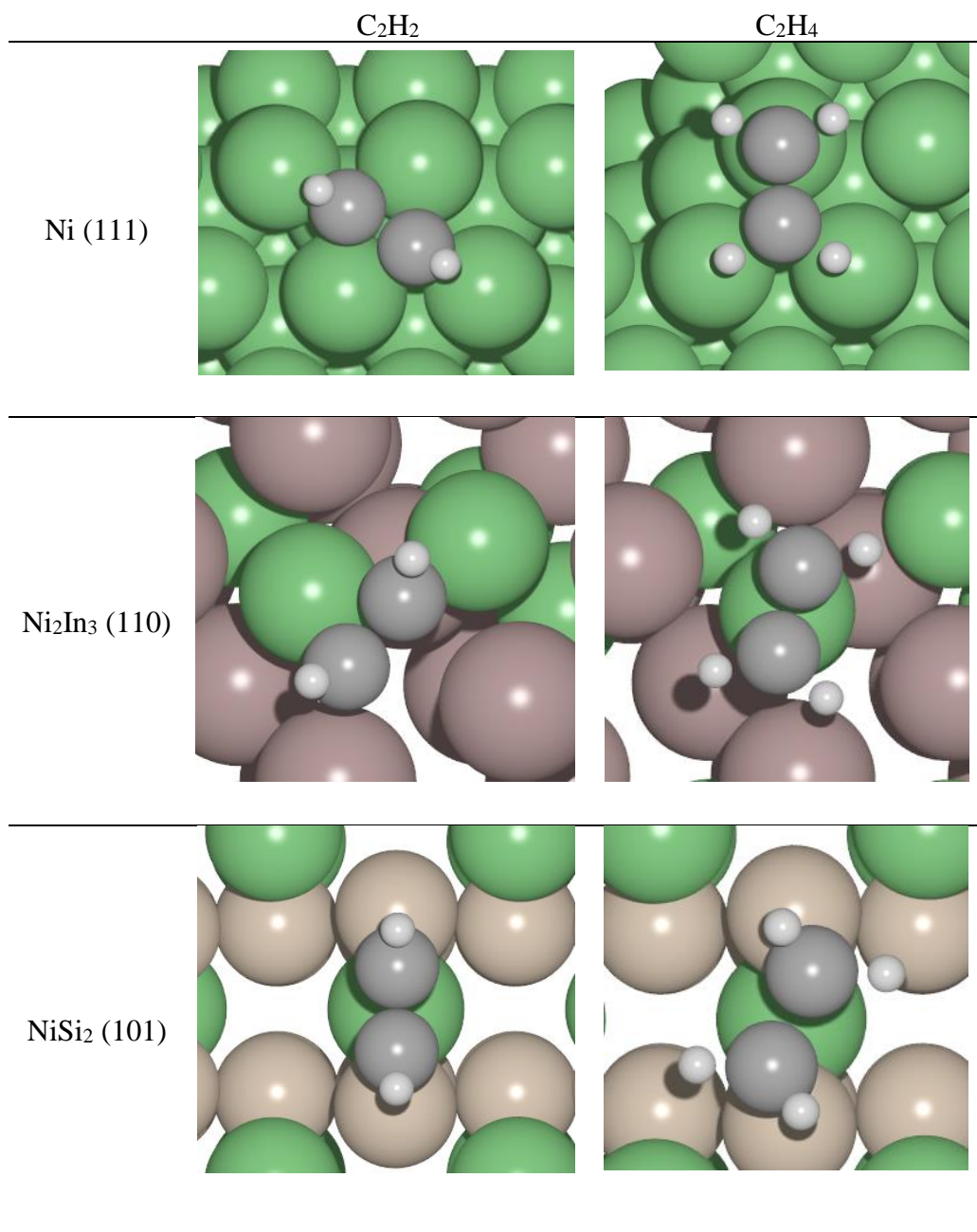
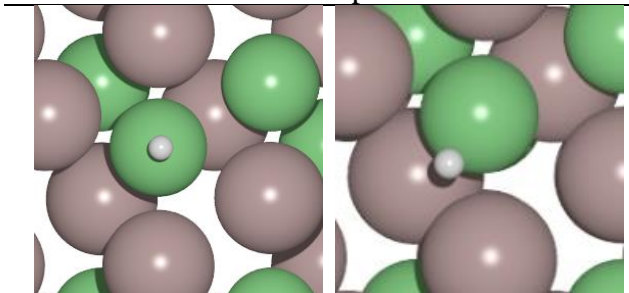


Figure 3.2: Most stable acetylene and ethylene configurations on Ni (111),  $Ni_2In_3$  (110) and  $NiSi_2$  (101).

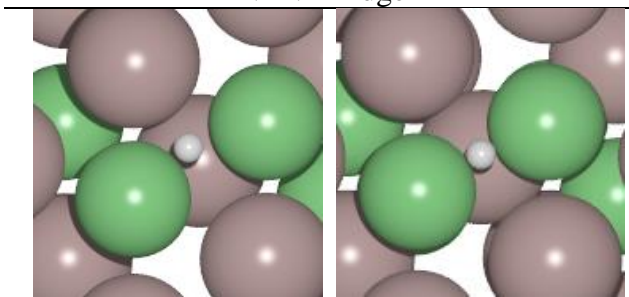


Before Optimization      After Optimization

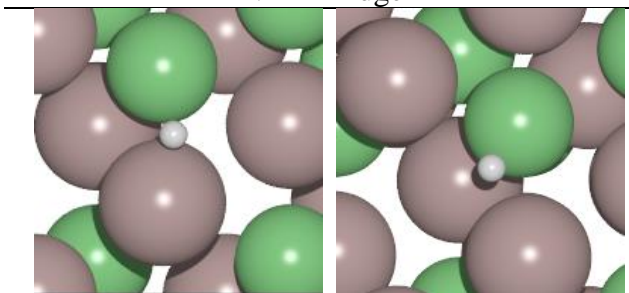
Ni Top



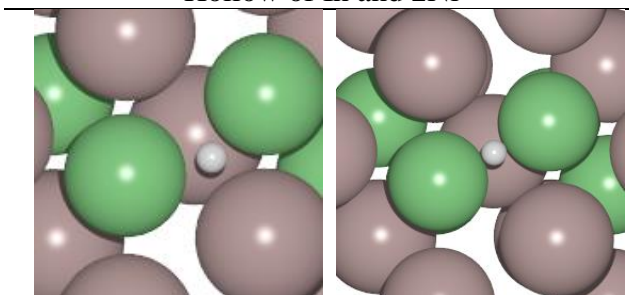
Ni-Ni Bridge



Ni-In Bridge



Hollow of In and 2Ni



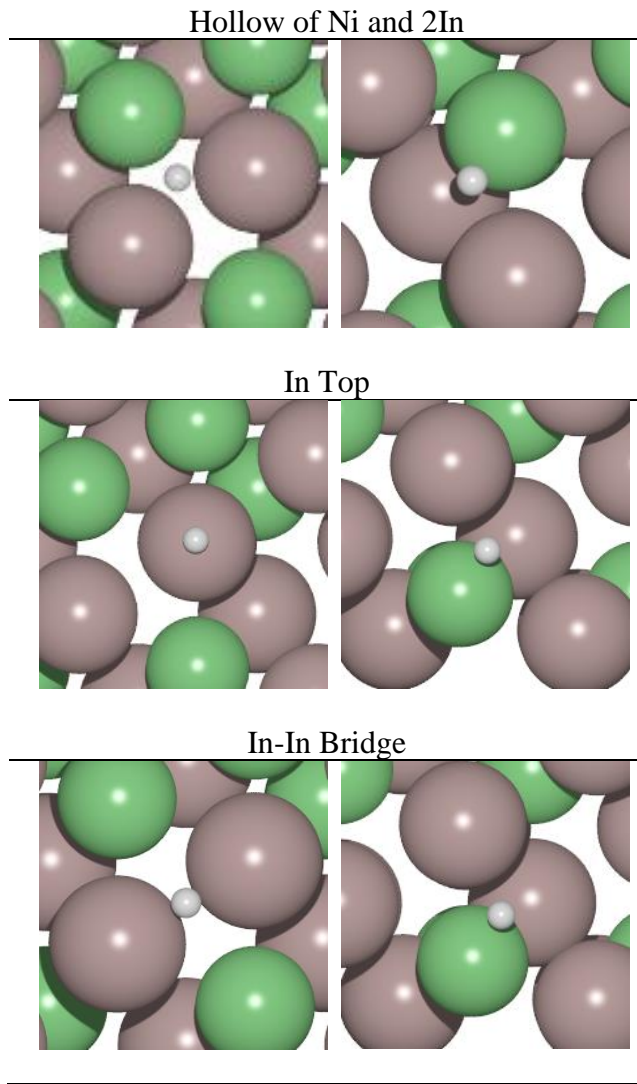


Figure 3.3: Hydrogen adsorption sites on  $\text{Ni}_2\text{In}_3$  (110) surface before and after optimization.

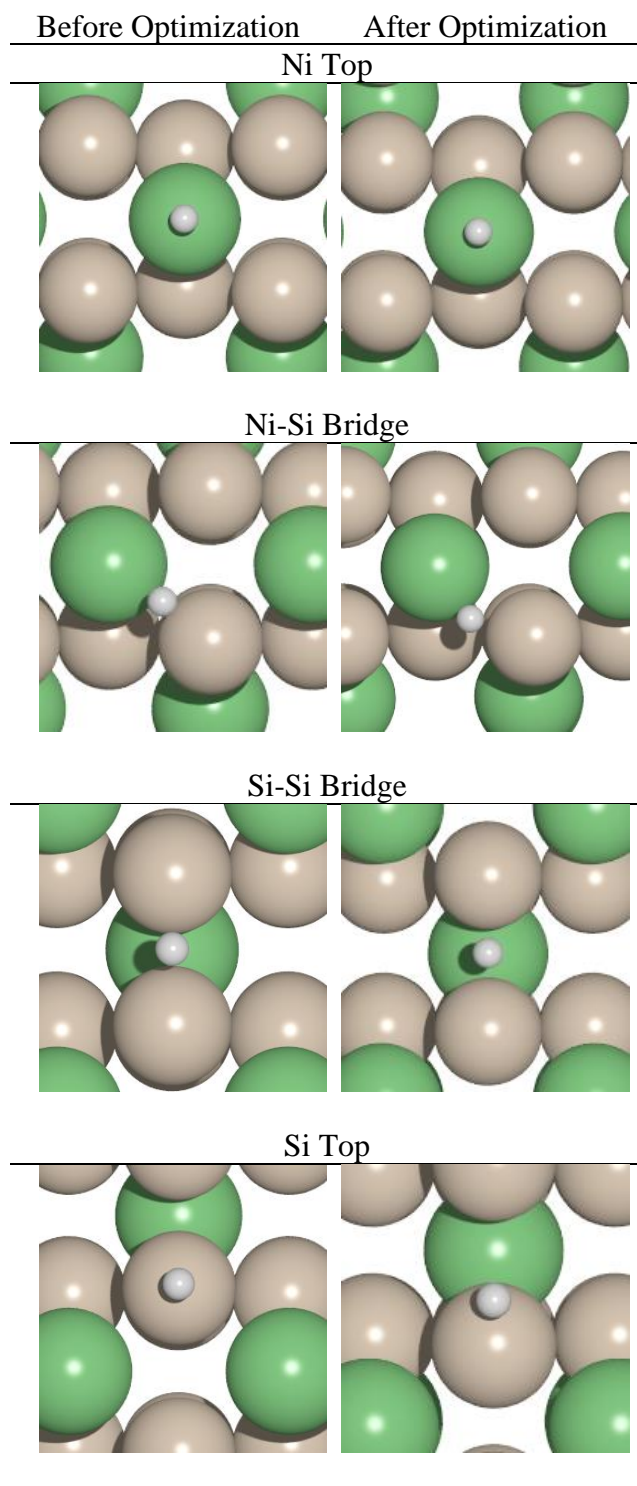


Figure 3.4: Hydrogen adsorption sites on NiSi<sub>2</sub> (101) before and after optimization.

### 3.3 Thermochemical Analysis

Thermochemical analysis was done to confirm the calculated values of the free unreacted gaseous molecules: hydrogen, acetylene, ethylene, and ethane. Potential energy of acetylene and hydrogen gas were used as reference values for calculating all the reaction energies in the hydrogenation and oligomerization reaction profiles. Table 3.8 presents the thermochemical analysis of the adsorbate gaseous molecules calculated using GGA-PBE and DFT-D3. No significant difference between the values obtained by GAA-PBE and DFT-D3 for hydrogen and acetylene, while values of ethylene and ethane had around 0.01 and 0.03 eV difference, respectively. Overall, values calculated using DFT-D3 are expected to deviate from GGA-PBE values when molecular weight increases. Zero-point vibrational energy was included in the calculations as per equation (3.3).

$$E_{ZPE} = \sum_i \frac{h\nu_i}{2} \quad (3.3)$$

Where  $E_{ZPE}$  is the zero-point energy,  $h$  is Planck's constant and  $\nu_i$  are vibrational frequencies.

Heat of enthalpy  $\Delta H$  of ethylene and ethane formation was calculated and compared to values in the literature as shown in Table 3.9. More negative values were obtained using DFT-D3 in comparison to GGA-PBE. This pattern was also observed when calculating the bulk lattice parameters shown in Table 2.3. Calculations were done under standard conditions at 25°C and 1 atm.

Table 3.8: Thermochemical analysis for free gaseous molecules in the hydrogenation reaction calculated using GGA-PBE and DFT-D3 methods.

GGA-PBE	$E_{\text{potential}}$ eV	$E_{\text{zpe}}$ eV	H eV	G eV
H <sub>2</sub>	-6.76	0.27	-6.40	-6.81
C <sub>2</sub> H <sub>2</sub>	-22.95	0.71	-22.13	-22.75
C <sub>2</sub> H <sub>4</sub>	-31.97	1.35	-30.51	-31.19
C <sub>2</sub> H <sub>6</sub>	-40.49	1.79	-38.58	-39.29
DFT-D3	$E_{\text{potential}}$ eV	$E_{\text{ZPE}}$ eV	H eV	G eV
H <sub>2</sub>	-6.76	0.27	-6.40	-6.81
C <sub>2</sub> H <sub>2</sub>	-22.95	0.71	-22.13	-22.75
C <sub>2</sub> H <sub>4</sub>	-31.98	1.35	-30.52	-31.20
C <sub>2</sub> H <sub>6</sub>	-40.52	1.79	-38.61	-39.31

Table 3.9: Enthalpy  $\Delta H$  of ethylene and ethane formation calculated using GGA-PBE and DFT-D3 and compared to experimental literature values (2).

GGA-PBE	$\Delta H$ kJ/mol	Experimental Value kJ/mol	Difference kJ/mol
$H_2 + C_2H_2 \rightarrow C_2H_4$	-190.66	-172	-18.66
$H_2 + C_2H_4 \rightarrow C_2H_6$	-124.76	-136	11.24
$2H_2 + C_2H_2 \rightarrow C_2H_6$	-315.41	-308	-7.41
DFT-D3			
$H_2 + C_2H_2 \rightarrow C_2H_4$	-191.52	-172	-19.52
$H_2 + C_2H_4 \rightarrow C_2H_6$	-126.01	-136	9.99
$2H_2 + C_2H_2 \rightarrow C_2H_6$	-317.53	-308	-9.53

## CHAPTER 4

### Acetylene Hydrogenation Reaction Profiles

The first step in the hydrogenation pathway was C-H bond formation with the adsorbed acetylene molecule producing vinyl. Vinyl was further hydrogenated to form ethylene. Ethylene would either desorb from the surface or over hydrogenate and form ethane. An active catalyst should have low adsorption and hydrogenation barrier for acetylene. A selective catalyst should have a small ethylene desorption barrier and a high hydrogenation barrier to avoid over hydrogenation.

The hydrogenation reaction profiles are shown in Figure 4.1 and Figure 4.2. Ni (111) hydrogenation reaction profile was consistent with the previous studies (6)(11). The reaction profiles started with acetylene adsorption on the surface following the Horiuti–Polanyi mechanism (2)(11). The first two activation energies in the reaction profile indicate the activity of the surface. The largest activation energy in the hydrogenation reaction profiles for Ni (111) and NiSi<sub>2</sub> (101) was obtained during ethylene hydrogenation. While vinyl hydrogenation has the largest activation energy on Ni<sub>2</sub>In<sub>3</sub> (110). No significant change in energy level was observed during the addition of H atom on NiSi<sub>2</sub> (101). This could be attributed to the low adsorption of H atoms as shown in Table 3.7. Overall, the hydrogenation reaction profile for Ni<sub>2</sub>In<sub>3</sub> (110) and NiSi<sub>2</sub> (101) exhibited different trends than Ni (111) due to the applied “geometric effect” and “electronic effect”.

Table 4.1 presents the adsorption energy and hydrogenation barrier of acetylene on Ni (111), Ni<sub>2</sub>In<sub>3</sub> (110), and NiSi<sub>2</sub> (101). No correlation was observed between the adsorption energy and the hydrogenation barrier of acetylene. Ni (111) and Ni<sub>2</sub>In<sub>3</sub> (110) had close acetylene hydrogenation barriers, while NiSi<sub>2</sub> (101) showed an increase of approximately 0.3 eV compared to Ni (111). The

strong adsorption of acetylene over Ni (111) and NiSi<sub>2</sub> (101) could block hydrogen molecules from adsorbing on the surface.

Selectivity can be evaluated through the ethylene desorption barriers and hydrogenation barriers presented in Table 4.2. These values were calculated according to equation (4.1) and equation (4.2). All three surfaces exhibited less than 0.2 eV difference between desorption and hydrogenation indicating that ethane formation was very likely. Despite the weak adsorption of acetylene and ethylene on the Ni<sub>2</sub>In<sub>3</sub> (110), the selectivity of the catalyst toward ethylene was not enhanced. This came in agreement with reported experiments about finding an optimum Ni/In ratio, that would enhance the selectivity while sustaining the activity of the catalyst (4)(25). Therefore, adsorption energy alone was not an accurate descriptor of surface selectivity. NiSi<sub>2</sub> (101) adsorbed acetylene and ethylene strongly and showed increased selectivity toward ethylene. The effect was analogous to the reported Si effect on Pd-Si catalysts. Si played a part in enhancing selectivity toward ethylene, while acetylene hydrogenation activity was slightly lower than pure transition metal catalysts (15).

Table 4.3 shows ethane desorption barriers on Ni (111), Ni<sub>2</sub>In<sub>3</sub> (110), and NiSi<sub>2</sub> (101). Monometallic Ni had a significantly higher ethane desorption barrier compared to Ni<sub>2</sub>In<sub>3</sub> (110) and NiSi<sub>2</sub> (101). In general, ethane showed very weak adsorption to the reaction surfaces, so that it would readily desorb. Table 4.4 shows the C-H bond distance in the initial state and the transition state of each extrema in the hydrogenation pathway. The C-H bond distance of all the transition states fell within the expected range of 1.2~1.9 Å (11) (23). Structures of the initial states, transition states, and final states on Ni (111), Ni<sub>2</sub>In<sub>3</sub> (110), and NiSi<sub>2</sub> (101) are shown in Figure 4.3, Figure 4.4, and Figure 4.5. Figure 4.4 shows C<sub>2</sub> molecules were activated around Ni atoms indicating that Ni atoms were the prime active sites on the surface. On the contrary, Figure 4.5 shows C<sub>2</sub>



molecules were activated even when they were not bonding with Ni atoms indicating that Ni atoms were not the only active sites on the surface.

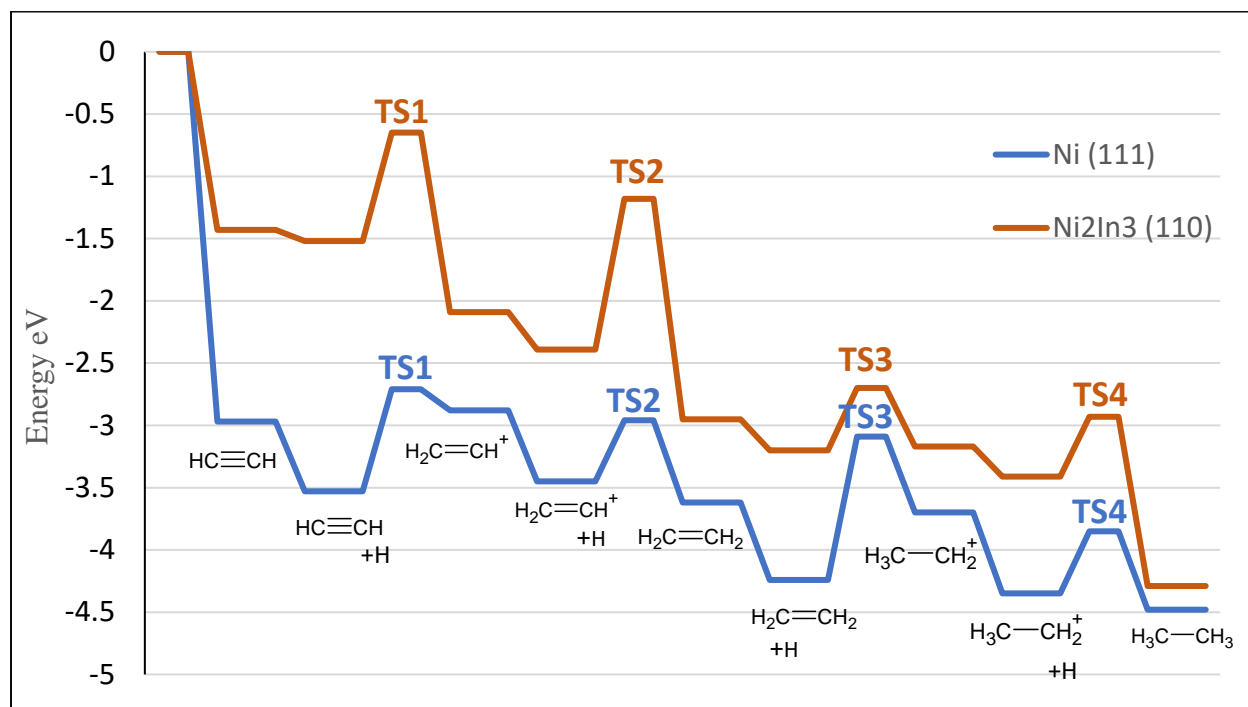


Figure 4.1: Acetylene hydrogenation reaction profile on Ni<sub>2</sub>In<sub>3</sub> (110) and monometallic Ni catalysts.

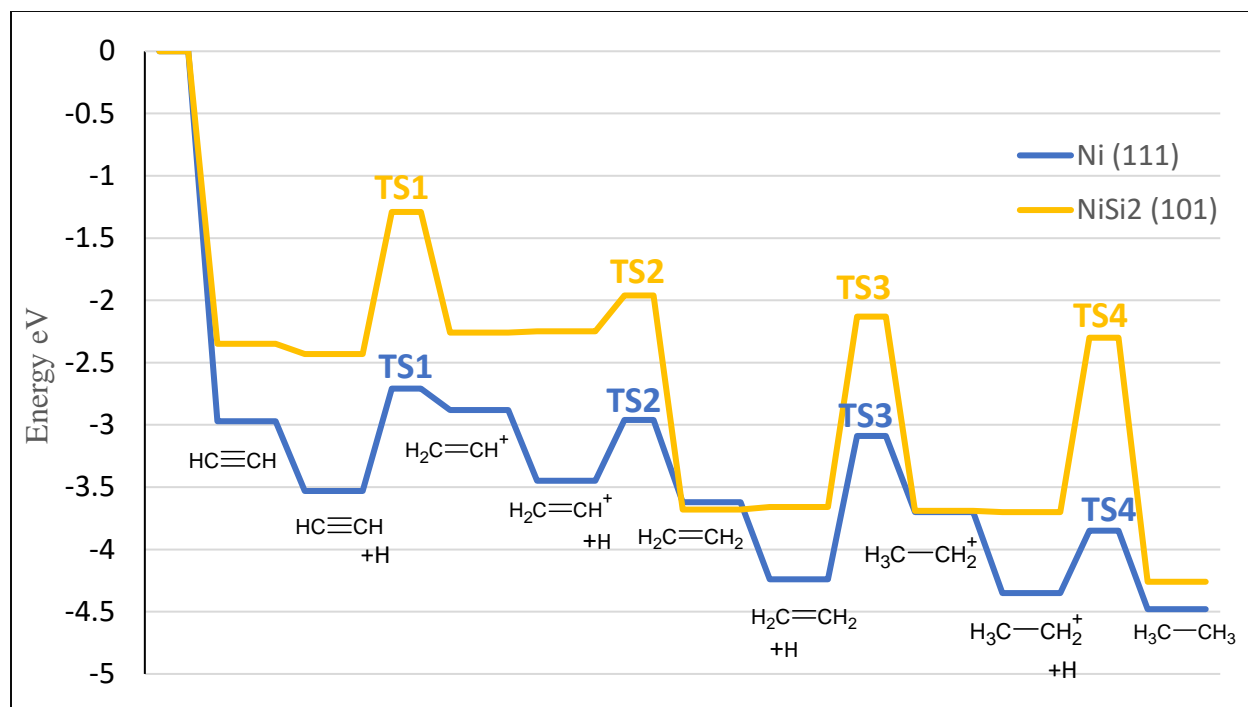


Figure 4.2: Acetylene hydrogenation reaction profile on NiSi<sub>2</sub> (101) and monometallic Ni catalysts.

$$E_{\text{desorption barrier}} = E_{\text{adsorbed ethylene}} - E_{\text{ethylene}(g)} - E_{\text{acetylene}(g)} - E_{\text{hydrogen}(g)} \quad (4.1)$$

$$E_{\text{hydrogenation barrier}} = E_{\text{initial state}} - E_{\text{transition state}} \quad (4.2)$$

Table 4.1: Acetylene adsorption energy and hydrogenation barrier (eV) on Ni (111), Ni<sub>2</sub>In<sub>3</sub> (110), and NiSi<sub>2</sub> (101).

	Adsorption Energy eV	Hydrogenation Barrier eV
Ni (111)	-2.97	0.82
Ni <sub>2</sub> In <sub>3</sub> (110)	-1.43	0.87
NiSi <sub>2</sub> (101)	-2.35	1.14

Table 4.2: Ethylene desorption barrier (eV), ethylene hydrogenation barrier (acetylene over-hydrogenation barrier) (eV) on Ni (111), Ni<sub>2</sub>In<sub>3</sub> (110), and NiSi<sub>2</sub> (101).

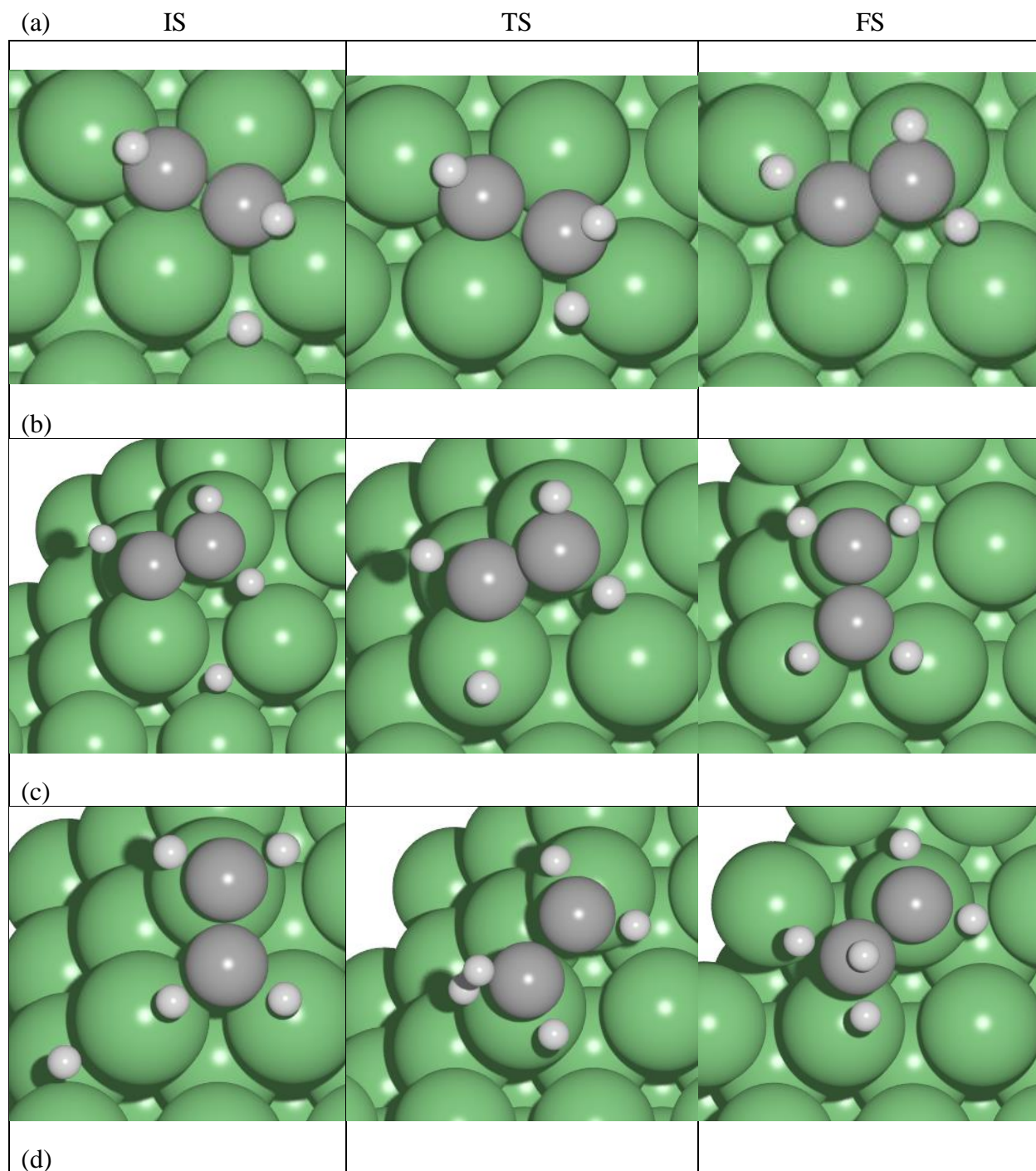
	Desorption Barrier eV	Hydrogenation Barrier eV
Ni (111)	1.34	1.15
Ni <sub>2</sub> In <sub>3</sub> (110)	0.68	0.50
NiSi <sub>2</sub> (101)	1.41	1.53

Table 4.3: Ethane desorption barrier (eV) on Ni (111), Ni<sub>2</sub>In<sub>3</sub> (110), and NiSi<sub>2</sub> (101).

Desorption Barrier eV	
Ni (111)	0.43
Ni <sub>2</sub> In <sub>3</sub> (110)	0.24
NiSi <sub>2</sub> (101)	0.20

Table 4.4: Distance (Å) between bonding C and H atoms from the initial state (IS) to the transition state (TS) on Ni (111), Ni<sub>2</sub>In<sub>3</sub> (110), and NiSi<sub>2</sub> (101).

	C <sub>2</sub> H <sub>2</sub> +H → C <sub>2</sub> H <sub>3</sub>		C <sub>2</sub> H <sub>3</sub> +H → C <sub>2</sub> H <sub>4</sub>		C <sub>2</sub> H <sub>4</sub> +H → C <sub>2</sub> H <sub>5</sub>		C <sub>2</sub> H <sub>5</sub> +H → C <sub>2</sub> H <sub>6</sub>	
	IS	TS	IS	TS	IS	TS	IS	TS
Ni (111)	2.048	1.238	2.608	1.767	3.201	1.480	2.500	1.600
Ni <sub>2</sub> In <sub>3</sub> (110)	2.678	1.755	2.601	1.484	2.554	1.423	2.765	1.745
NiSi <sub>2</sub> (101)	2.745	1.446	2.899	1.950	2.767	1.425	2.817	1.528



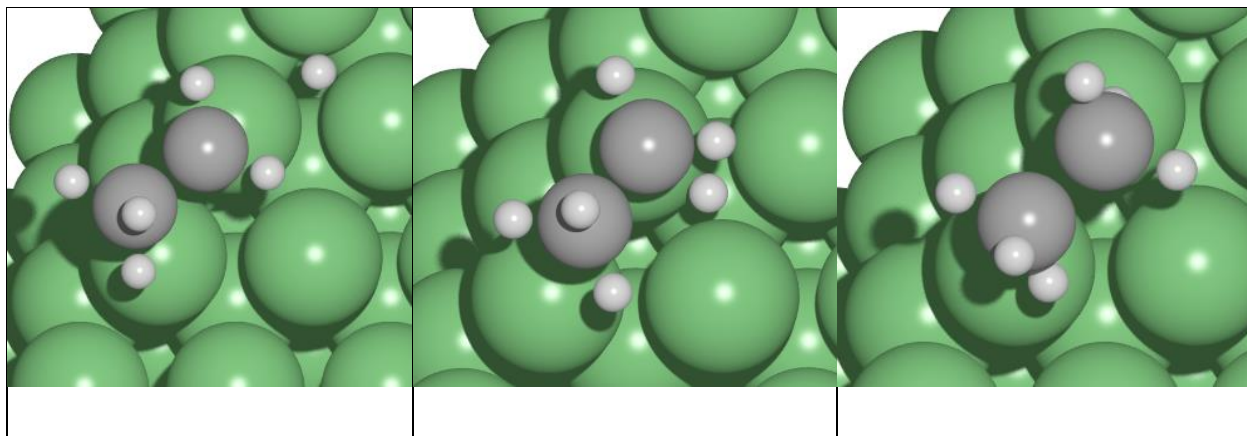
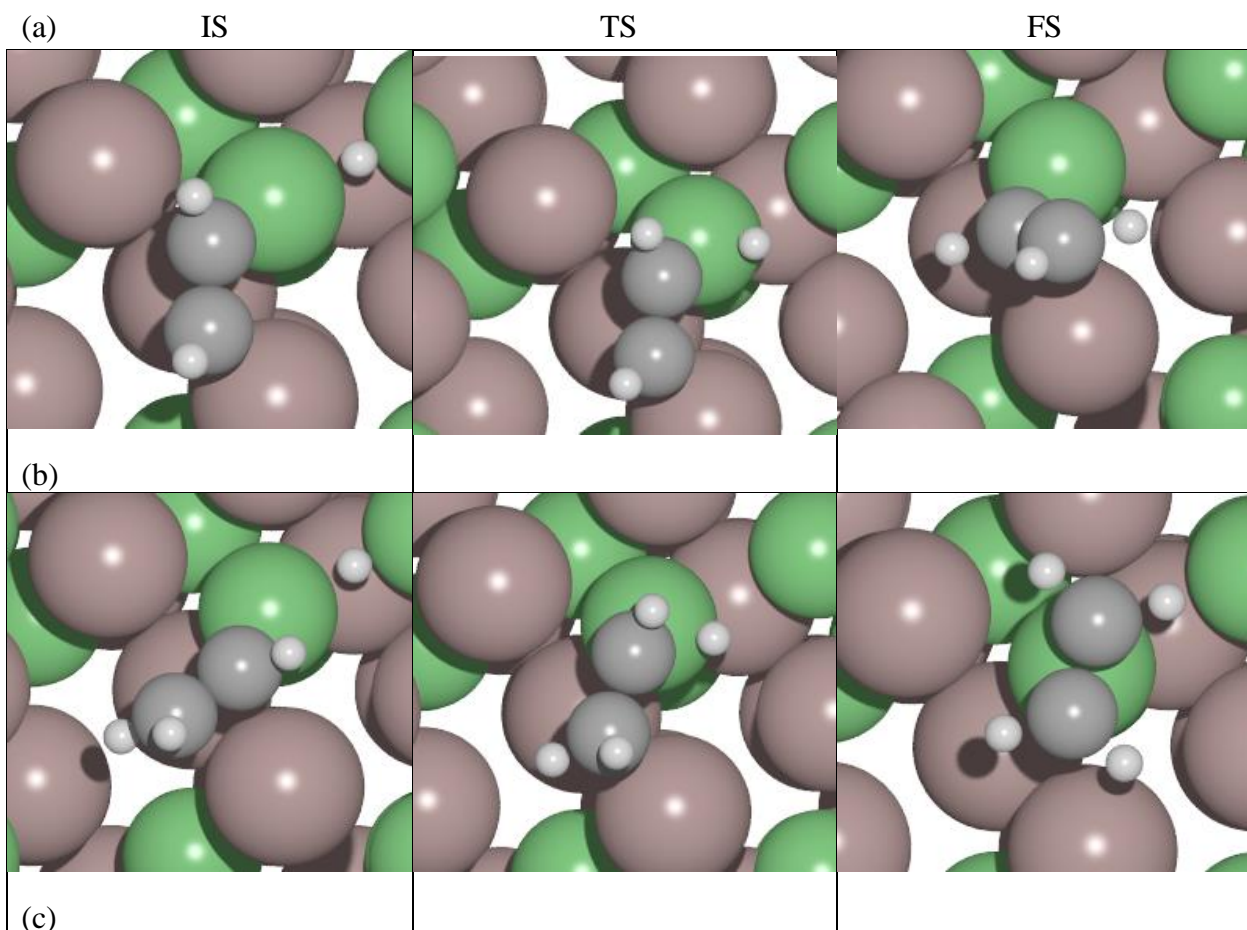


Figure 4.3: Structures of transition states in acetylene hydrogenation pathway on Ni (111): (a) Hydrogenation of adsorbed acetylene to form vinyl. (b) Vinyl hydrogenation to form ethylene. (c) Ethylene hydrogenation to form  $C_2H_5$ . (d) Hydrogenation of  $C_2H_5$  to form ethane. IS: initial state, TS: transition state, FS: final state.



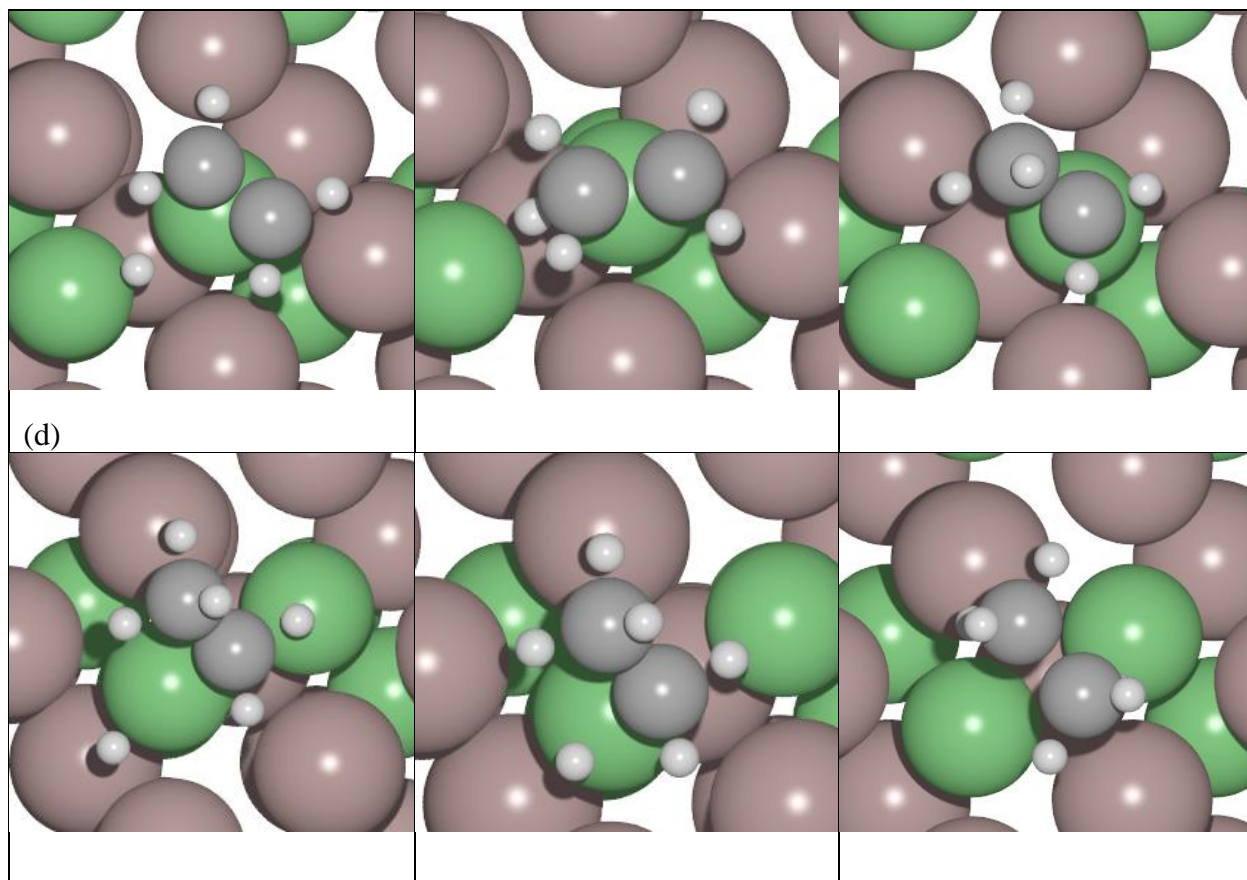
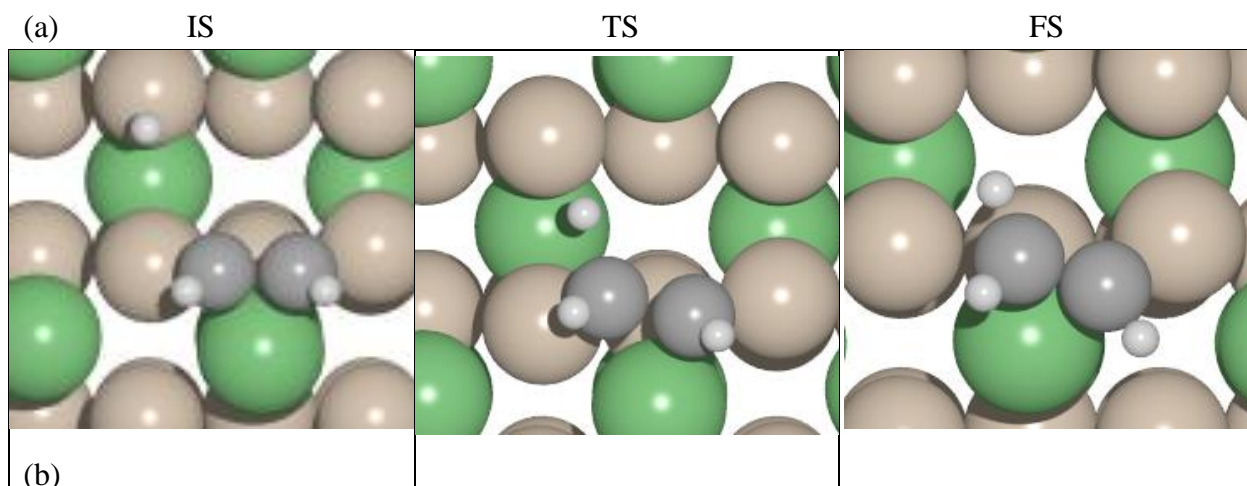


Figure 4.4: Structures of transition states in acetylene hydrogenation pathway on  $\text{Ni}_2\text{In}_3$  (110):

(a) Hydrogenation of adsorbed acetylene to form vinyl. (b) Vinyl hydrogenation to form ethylene. (c) Ethylene hydrogenation to form  $\text{C}_2\text{H}_5$ . (d) Hydrogenation of  $\text{C}_2\text{H}_5$  to form ethane.

IS: initial state, TS: transition state, FS: final state.



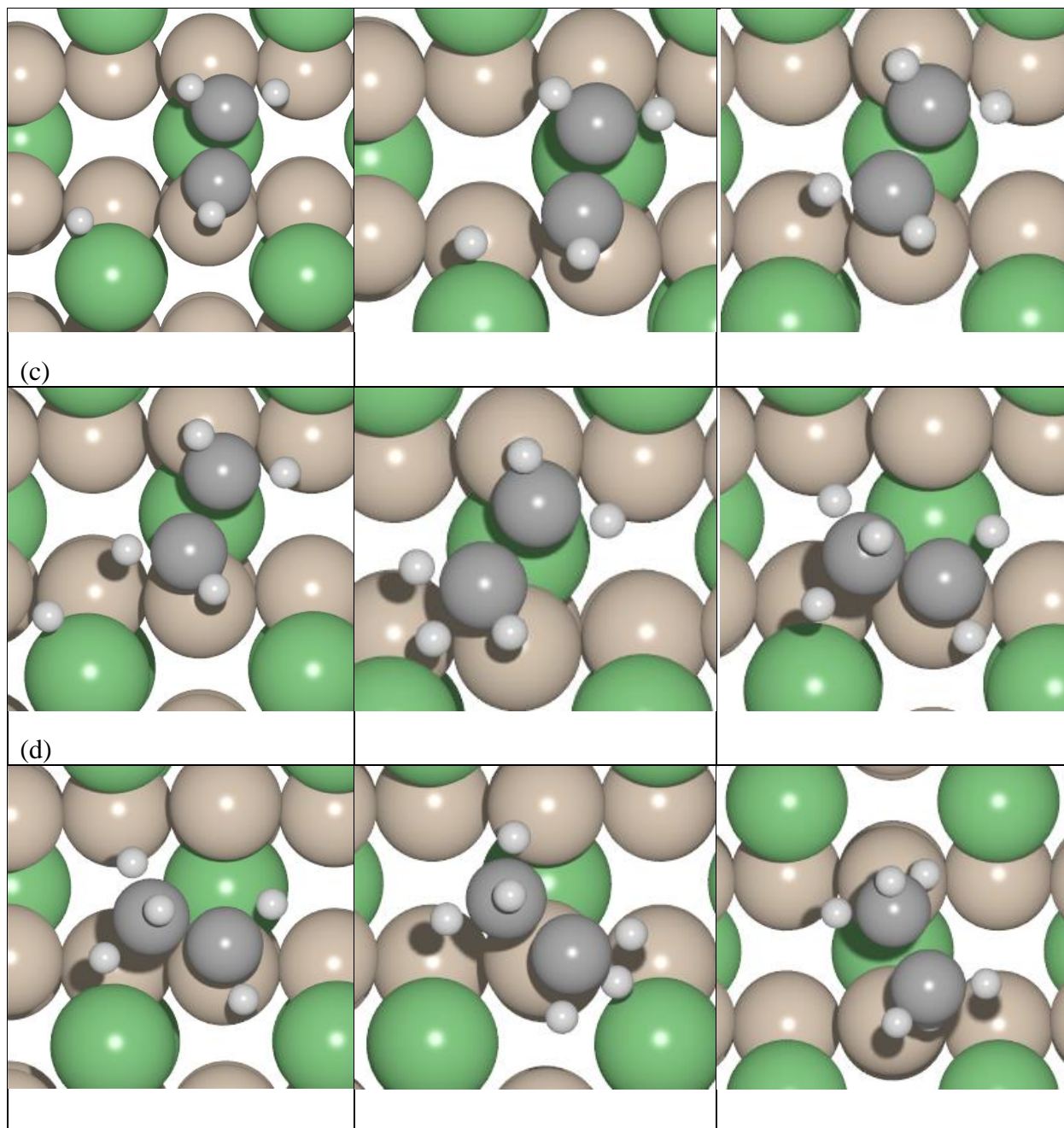


Figure 4.5: Structures of transition states in acetylene hydrogenation pathway on  $\text{NiSi}_2$  (101): (a) Hydrogenation of adsorbed acetylene to form vinyl. (b) Vinyl hydrogenation to form ethylene. (c) Ethylene hydrogenation to form  $\text{C}_2\text{H}_5$ . (d) Hydrogenation of  $\text{C}_2\text{H}_5$  to form ethane. IS: initial state, TS: transition state, FS: final state.

## CHAPTER 5

### Acetylene Oligomerization Reaction Profiles

Acetylene oligomerization reaction is initiated through C-C coupling. While there were other possible reactions for C-C coupling between molecules such as acetylene, vinylidene, and vinyl, the literature agreed that the most kinetically favorable precursors for oligomers were acetylene and vinyl (5)(6). After forming C<sub>4</sub> hydrocarbon through C-C coupling, the hydrocarbon molecules would further hydrogenate to form butadiene. The oligomerization pathway had two transition states: C-C coupling to form C<sub>4</sub> hydrocarbon and C-H bond formation to produce butadiene. The C-C coupling transition state was a key step in considering the overall selectivity of the catalyst as it competed with the hydrogenation of acetylene and the formation of ethylene.

Figure 5.1 and Figure 5.2 show the reaction profiles of acetylene oligomerization starting by C-C bond formation between adsorbed acetylene and vinyl, followed by a hydrogenation step to produce 1,3-butadiene. The calculated Ni (111) oligomerization reaction profile was consistent with the previous studies (6). The largest activation energy in acetylene oligomerization reaction profiles for Ni (111) and NiSi<sub>2</sub> (101) was obtained during C-C bond formation. While C<sub>4</sub>H<sub>5</sub> hydrogenation was the largest activation energy on Ni<sub>2</sub>In<sub>3</sub> (110). The reaction profile of Ni<sub>2</sub>In<sub>3</sub> (110) had the same oligomerization trend of the IMC NiZn. In comparison to Ni (111), IMC NiZn had a lower energy barrier for C-C bonding and a high activation barrier for C<sub>4</sub>H<sub>5</sub> hydrogenation (6). On the other hand, Figure 5.2 shows that H adsorption with C<sub>4</sub>H<sub>5</sub> followed the same trend of H adsorption with C<sub>2</sub> molecules, and no change of energy was observed in the reaction profile upon H adsorption.



Table 5.1 compares the energy barrier for C-C coupling, acetylene adsorption, and vinyl reaction energy. Overall, no significant correlation was observed between acetylene adsorption or vinyl reaction energy and oligomers formation barrier among Ni (111), Ni<sub>2</sub>In<sub>3</sub> (110), and NiSi<sub>2</sub> (101). In comparison to Pd surfaces, on which C<sub>4</sub> hydrocarbon was stabilized by four Pd atoms (43), Ni<sub>2</sub>In<sub>3</sub> (110) showed C<sub>4</sub> hydrocarbon stability with only two isolated Ni atoms. Oligomers would form more readily on Ni<sub>2</sub>In<sub>3</sub> (110) in comparison to Ni (111). This could be attributed to the weak binding of the surface. The correlation between acetylene conversion and C<sub>4</sub> formation has been studied experimentally (4)(6)(15)(25). Spanjers et al. confirmed that acetylene conversion on Ni-based catalysts was inversely proportional to butadiene formation (6). Ni<sub>2</sub>In<sub>3</sub> (110) showed low conversion levels when tested experimentally for aldehydes hydrogenation (25). Experiments by Chen et al. showed substantial formation of C<sub>4</sub> hydrocarbons when Ni/In ratio was low (4). These studies gave insights about acetylene low conversion on Ni<sub>2</sub>In<sub>3</sub> (110) and were supported by the known competition between acetylene hydrogenation and acetylene oligomerization.

On the other hand, NiSi<sub>2</sub> (101) had a relatively high C-C coupling barrier and could result in a minimal level of oligomers formation. This result came in agreement with the literature, where the completely isolated Ni active sites would have a low risk of acetylene oligomerization (5)(44). It also came in a similar fashion to Si effect on Si-promoted Pd catalysts (15). Green oil formation was suppressed on Si-modified catalysts in comparison to pure transition metal catalysts. Overall, In and Si had a different influence on facilitating C-C coupling. While the overall selectivity of the Ni<sub>2</sub>In<sub>3</sub> (110) was compromised, the selectivity of the NiSi<sub>2</sub> (101) was improved by decreasing acetylene oligomerization.

Table 5.2 presents butadiene desorption energy barriers. A significantly high desorption barrier was observed with Ni (111). This large value indicated that butadiene was likely to go through

further reactions over Ni (111) and produce heavy oligomers. Ni<sub>2</sub>In<sub>3</sub> (110) was most likely to form oligomers because it had the smallest C-C bond formation energy barrier, but it also had the smallest butadiene desorption barrier.

Initial, transition, and final state structures of the acetylene oligomerization pathway on Ni (111), Ni<sub>2</sub>In<sub>3</sub> (110), and NiSi<sub>2</sub> (101) are presented in Figure 5.3, Figure 5.4, and Figure 5.5. Figure 5.4 shows C<sub>4</sub>H<sub>5</sub> bonding with Ni active sites indicating that Ni atoms were the prime active sites on the surface. Due to the low adsorption of hydrogen on In atoms, it was difficult to place the H atom around C<sub>4</sub>H<sub>5</sub> because Ni atoms were occupied as shown in Figure 5.4 (b). Table 5.3 presents the distances of initial and transition states between bonding C atoms and C4 hydrogenation of the acetylene oligomerization pathway. The longest transition state distance between atoms was observed during C<sub>4</sub>H<sub>5</sub> hydrogenation on Ni<sub>2</sub>In<sub>3</sub> (110) demonstrating the difficulty of adding the H atom due to the weak binding of the surface. Figure 5.5 shows that C<sub>4</sub>H<sub>5</sub> was activated on Ni and Si atoms indicating that Ni atoms were not the only active sites on the surface. Also, placing an H atom for C<sub>4</sub>H<sub>5</sub> hydrogenation was not difficult as the case for Ni<sub>2</sub>In<sub>3</sub> (110). Observations of different effects between Ni<sub>2</sub>In<sub>3</sub> (110) and NiSi<sub>2</sub> (101) on hydrogen co-adsorption with hydrocarbon molecules came in agreement with the data presented in Table 3.6 and Table 3.7.

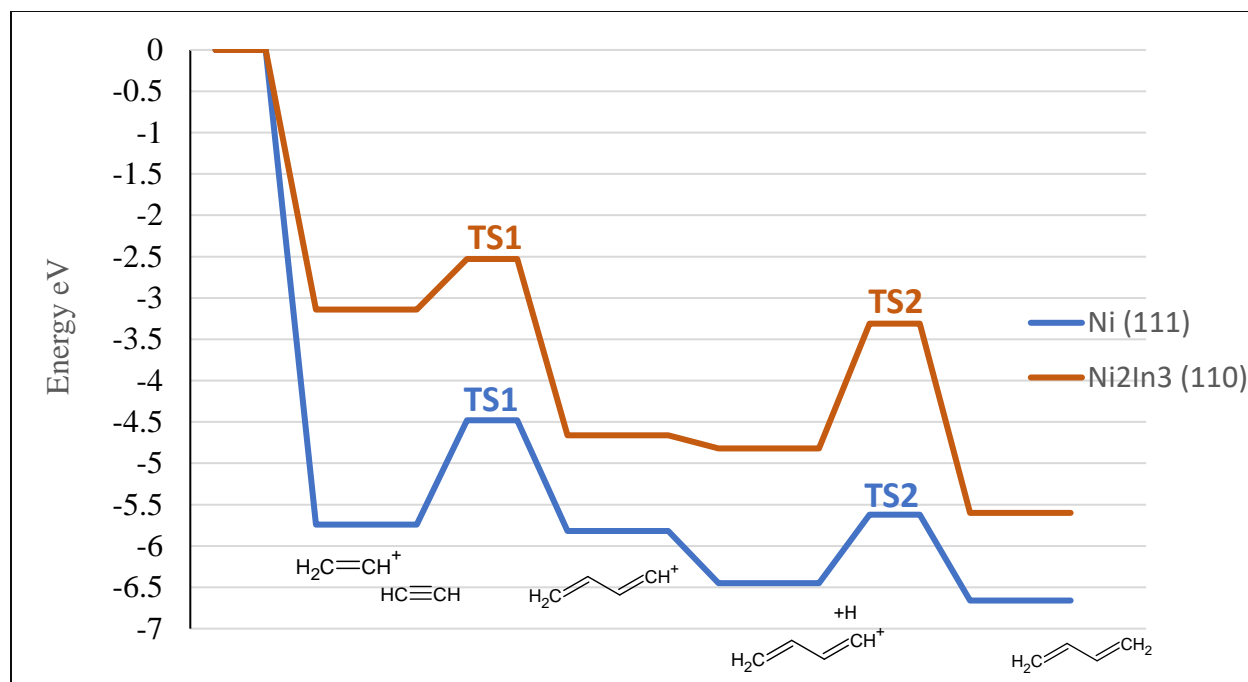


Figure 5.1: Acetylene oligomerization reaction profile of Ni<sub>2</sub>In<sub>3</sub> and monometallic Ni catalysts.

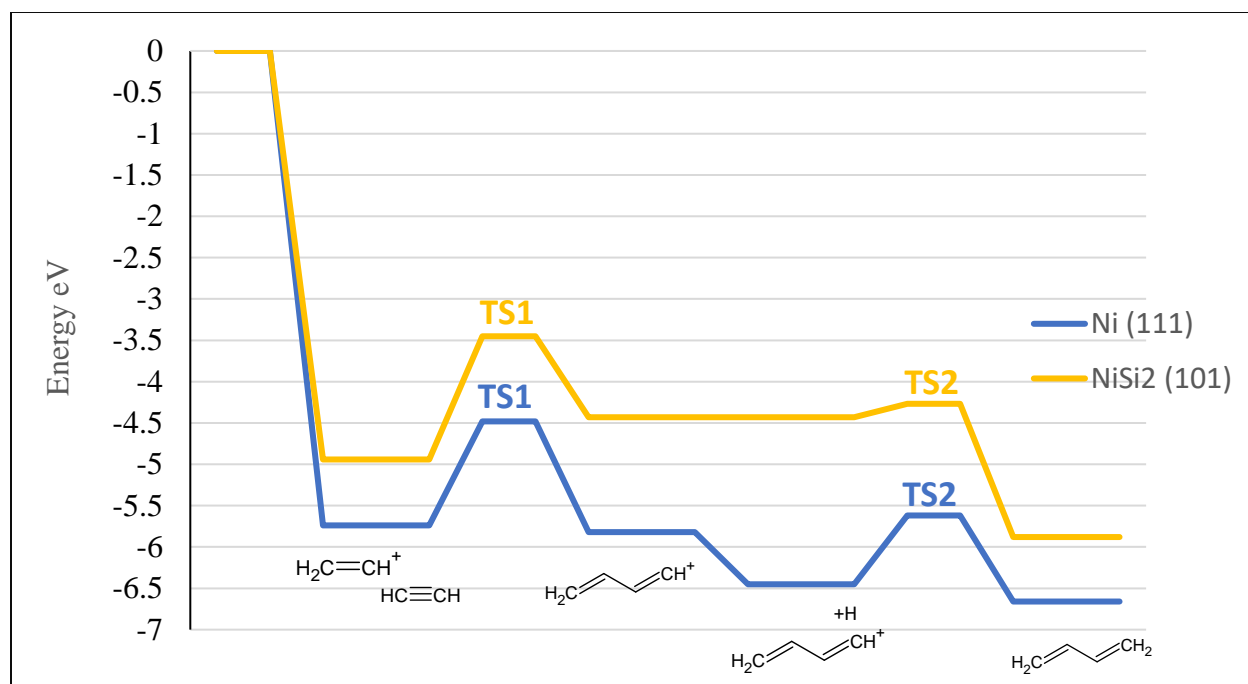


Figure 5.2: Acetylene oligomerization reaction profile of NiSi<sub>2</sub> and monometallic Ni catalysts.

Table 5.1: Comparison between the energy barrier (eV) of C-C coupling of acetylene and vinyl and the acetylene adsorption energy (eV) on Ni (111), Ni<sub>2</sub>In<sub>3</sub> (110), and NiSi<sub>2</sub> (101).

	C-C Coupling Barrier eV	Acetylene Adsorption eV	Vinyl Reaction Energy eV
Ni (111)	1.26	-2.97	-2.88
Ni <sub>2</sub> In <sub>3</sub> (110)	0.61	-1.43	-2.09
NiSi <sub>2</sub> (101)	1.49	-2.35	-2.26

Table 5.2: Butadiene desorption energy barrier (eV) calculated based on butadiene molecule desorption energy -4.42 (eV) on Ni (111), Ni<sub>2</sub>In<sub>3</sub> (110), and NiSi<sub>2</sub> (101).

	Butadiene Reaction Energy eV	Butadiene Desorption Barrier eV
Ni (111)	-6.66	2.24
Ni <sub>2</sub> In <sub>3</sub> (110)	-5.60	1.18
NiSi <sub>2</sub> (101)	-5.88	1.46

Table 5.3: Initial state (IS) and transition state (TS) distance (Å) between two C bonding to form C<sub>4</sub>H<sub>5</sub>, and between attacking H and C atom in subsequent hydrogenation to form C<sub>4</sub>H<sub>6</sub>.

	C <sub>2</sub> H <sub>2</sub> +C <sub>2</sub> H <sub>3</sub> → C <sub>4</sub> H <sub>5</sub>		C <sub>4</sub> H <sub>5</sub> +H → C <sub>4</sub> H <sub>6</sub>	
	IS	TS	IS	TS
Ni (111)	4.133	1.963	2.892	1.721
Ni <sub>2</sub> In <sub>3</sub> (110)	2.907	1.986	3.042	2.104
NiSi <sub>2</sub> (101)	2.785	2.036	2.794	1.937

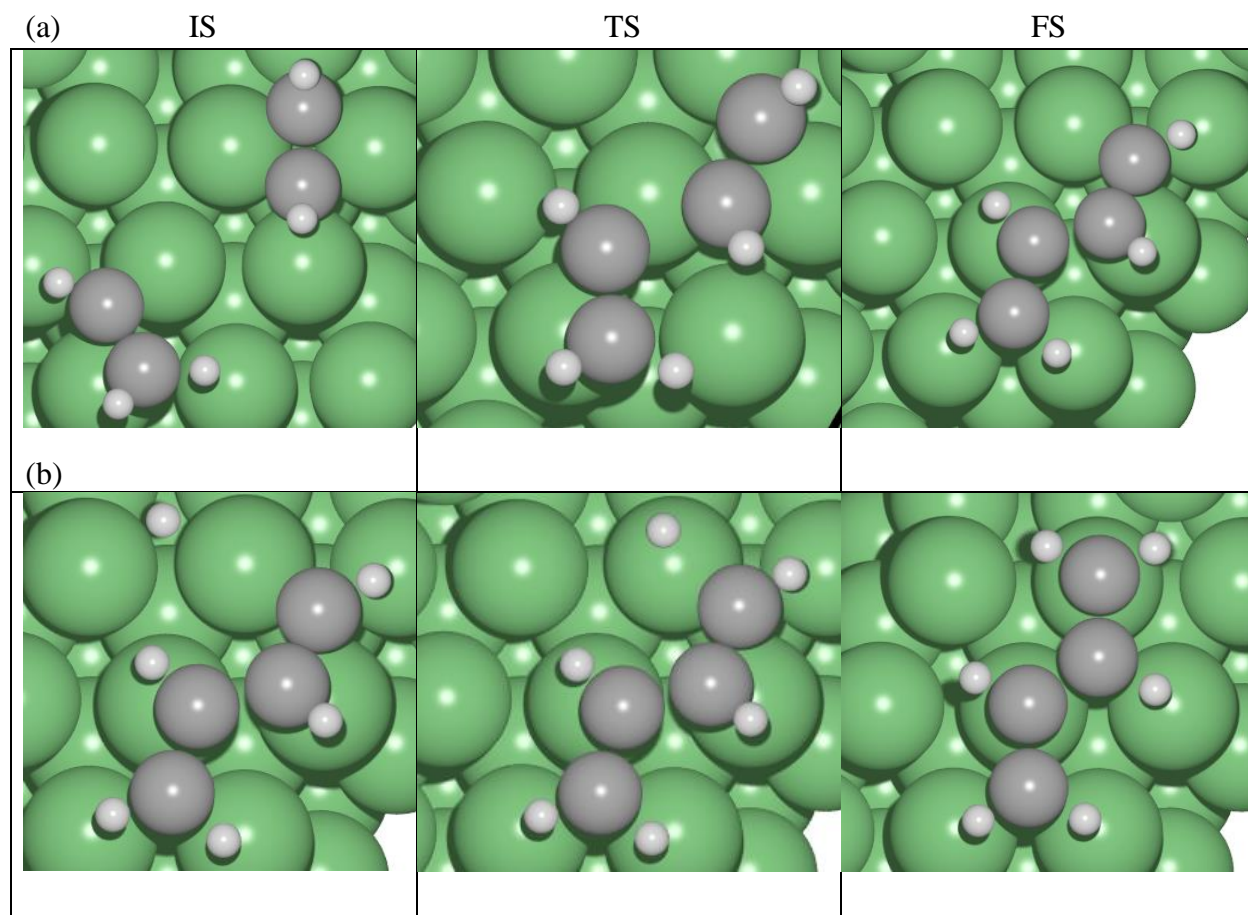


Figure 5.3: Structures of transition states for the acetylene oligomerization pathway on Ni (111):

(a) C-C bond formation between adsorbed acetylene and vinyl molecules. (b) Hydrogenation of adsorbed  $C_4H_5$  to form butadiene. IS: initial state, TS: transition state, FS: final state.

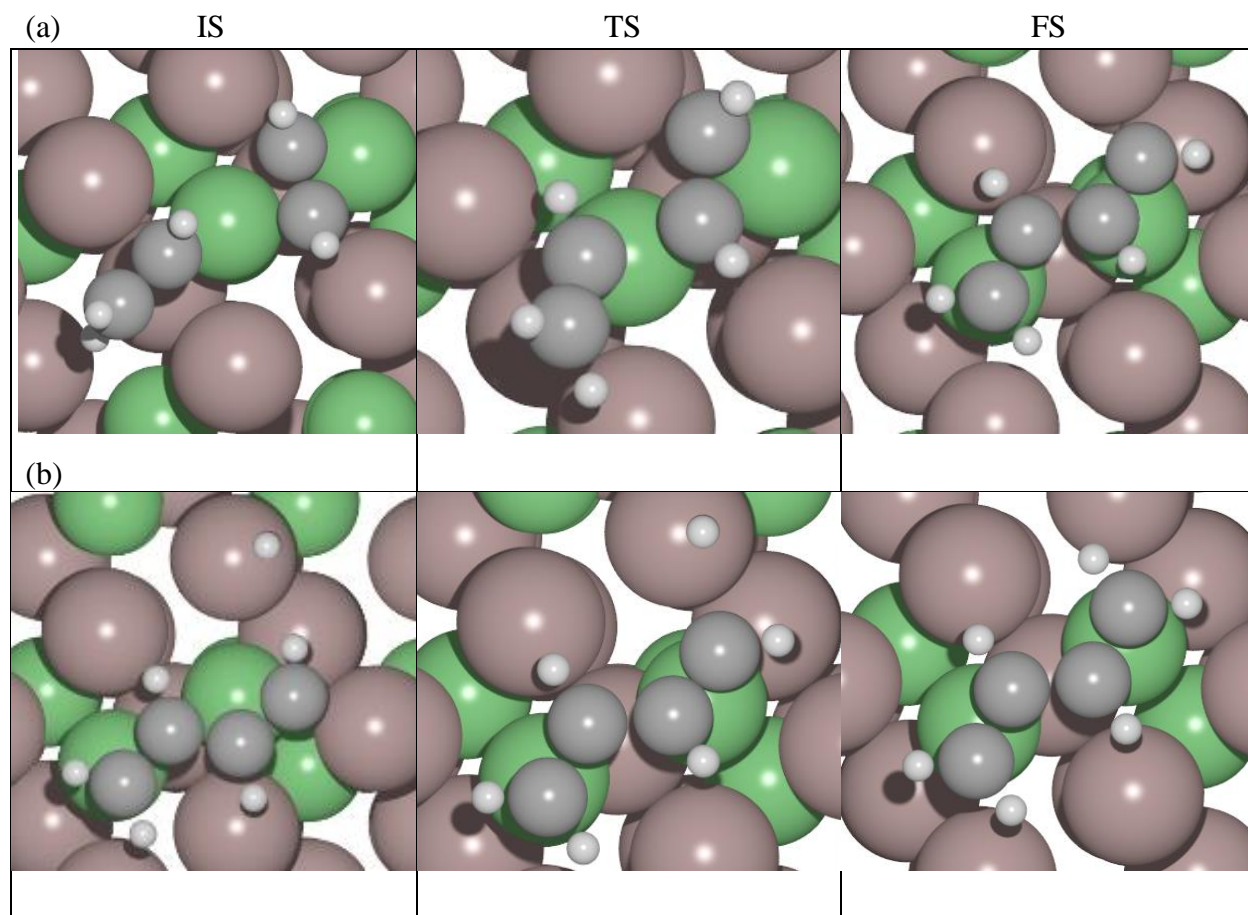


Figure 5.4: Structures of transition states for the acetylene oligomerization pathway on  $\text{Ni}_2\text{In}_3$

(110): (a) C-C bond formation between absorbed acetylene and vinyl molecules. (b)

Hydrogenation of absorbed  $\text{C}_4\text{H}_5$  to form butadiene. IS: initial state, TS: transition state, FS: final state.

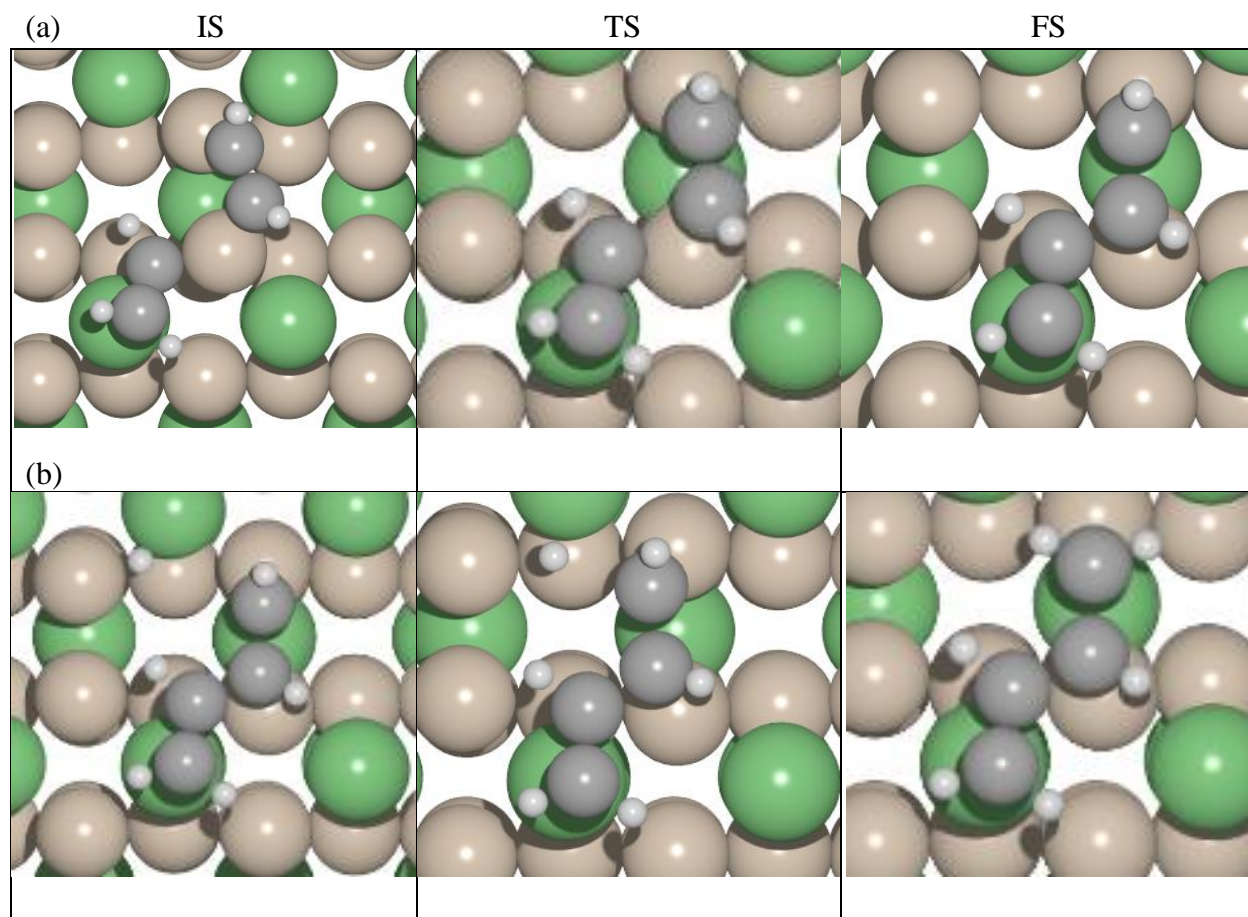


Figure 5.5: Structures of transition states for the acetylene oligomerization pathway on NiSi<sub>2</sub>

(101): (a) C-C bond formation between adsorbed acetylene and vinyl molecules. (b)

Hydrogenation of adsorbed C<sub>4</sub>H<sub>5</sub> to form butadiene. IS: initial state, TS: transition state, FS: final state.

## CHAPTER 6

### Conclusion and Future Work

IMC formulations of  $\text{Ni}_2\text{In}_3$  and  $\text{NiSi}_2$  were selected from their corresponding phase diagrams to investigate the case of partially and completely isolated Ni atoms in  $\text{Ni}_2\text{In}_3$  and  $\text{NiSi}_2$ , respectively. Bulk unit cell calculations and thermochemical analysis were performed using GGA-PBE and DFT-D3. Calculations were continued using DFT-D3 due to the nature of the chemical bonds between the gaseous adsorbates and the surfaces in this reaction. Surface energies of  $\text{Ni}_2\text{In}_3$  and  $\text{NiSi}_2$  facets were calculated. Symmetry on  $\text{NiSi}_2$  surface reduced the number of studied surfaces to two facets only, while  $\text{Ni}_2\text{In}_3$  had a less symmetric nature with five distinguished facets. The most stable facets were determined to be  $\text{Ni}_2\text{In}_3$  (110) and  $\text{NiSi}_2$  (101).

Possible adsorption sites for reactants, intermediates, and products were explored on  $\text{Ni}_2\text{In}_3$  (110) and  $\text{NiSi}_2$  (101). Hydrogen adsorption was weaker on  $\text{Ni}_2\text{In}_3$  (110) and  $\text{NiSi}_2$  (101) in comparison to monometallic Ni catalysts. Hydrogen adsorption over the  $\text{Ni}_2\text{In}_3$  (110) surface happened on the same active sites as acetylene and ethylene which is consistent with the literature (6)(10). Positive H atom adsorption energies were obtained over all the adsorption sites of  $\text{NiSi}_2$  (101). However, H atom did not favor Ni sites over Si sites as was the case in  $\text{Ni}_2\text{In}_3$  (110). Acetylene and ethylene were also most stable over “Ni-Ni Bridge” and “Hollow of In and 2Ni”. The most stable site for acetylene and ethylene adsorption on  $\text{NiSi}_2$  (101) was the “Si-Si bridge” site. By surveying the possible active sites on  $\text{Ni}_2\text{In}_3$  (110) and  $\text{NiSi}_2$  (101). It was found that hydrocarbon molecules on  $\text{NiSi}_2$  (101) were activated by Si and Ni atoms, while In atoms showed low binding activity toward hydrocarbon molecules.



The acetylene hydrogenation reaction profiles for Ni<sub>2</sub>In<sub>3</sub> (110) and NiSi<sub>2</sub> (101) exhibited different trends than Ni (111) due to the applied “geometric effect” and “electronic effect”. Selectivity was evaluated through the ethylene desorption and hydrogenation barriers. Despite the weak adsorption of acetylene and ethylene on the Ni<sub>2</sub>In<sub>3</sub> (110), the selectivity of the catalyst toward ethylene was not enhanced in comparison to Ni (111). NiSi<sub>2</sub> (101) adsorbed acetylene in a similar fashion to Ni (111). The strong adsorption of acetylene over Ni (111) and NiSi<sub>2</sub> (101) could block hydrogen molecules from adsorbing on the surface. However, NiSi<sub>2</sub> (101) had enhanced selectivity toward ethylene, while acetylene hydrogenation activity was slightly lower than Ni (111). These findings were consistent with the computational and experimental results in the literature.

Two neighboring Ni atoms on the Ni<sub>2</sub>In<sub>3</sub> (110) surface were enough to facilitate oligomers formation with a low energy barrier for C-C coupling. This could indicate that the catalyst had low acetylene conversion, because studies showed that C-C coupling and acetylene hydrogenation were inversely correlated (4)(6)(15)(25). On the other hand, the NiSi<sub>2</sub> (101) surface had the largest C-C coupling barrier even though it absorbed acetylene strongly. Butadiene desorption was not favorable on Ni (111) due to the large desorption barrier. This suggested that oligomerization was likely to proceed further to produce heavy molecules. Therefore, no direct correlation between acetylene adsorption energy and C-C coupling barrier could be drawn. Overall, the influence of adding a second metal to Ni could be correlated with enhancing the desorption of ethane and butadiene as evidenced in the case of Ni<sub>2</sub>In<sub>3</sub> (110) and NiSi<sub>2</sub> (101).

Exploring other phases of IMC with varied Ni/In and Ni/Si ratios may provide a better understanding of the optimum ratio of active transition metal to a second metal. Formulations with higher Ni content on the surface may also give insights about the active site ensemble that provides high selectivity while preserving the hydrogenation activity of the catalysts. Further investigation

of the “geometric effect” and the “electronic effect” in bimetallic systems could help in tuning the reaction toward the desired product. A more accurate selectivity descriptor that accounts for competitive oligomerization reaction is required particularly for Ni-based catalysts.

## APPENDIX

### 7.1 Adsorption Sites and Reaction Energies of Intermediates

Table 7.1: Adsorption sites of gaseous molecules over Ni<sub>2</sub>In<sub>3</sub> (110) surface.

Adsorption Site/ Adsorbed Molecule	Ni Top	Ni-Ni Bridge	Ni-In Bridge	Hollow of In and 2Ni	Hollow of Ni and 2In	In Top
CH <sub>2</sub> =CH	-1.84	-1.82	-1.83	-1.82	-2.09	-1.35
CH <sub>2</sub> =C	-1.53	-1.53	-1.53	-1.53	-1.00	-1.00
CH <sub>2</sub> CH <sub>3</sub>	-3.17	-3.08	-	-3.08	-	-

Table 7.2: Adsorption sites of gaseous molecules over NiSi<sub>2</sub> (101) surface.

Adsorption Site/ Adsorbed Molecule	Ni Top	Ni-Si Bridge	Si-Si Bridge	Si Top
CH <sub>2</sub> =C	-1.37	-0.50	-2.25	-1.37
CH <sub>2</sub> =CH	-1.66	-2.26	-2.05	-2.11
CH <sub>2</sub> CH <sub>3</sub>	-3.21	-3.58	-3.69	-3.68

## 7.2 Hydrogen Adsorption Sites and Reaction Energies

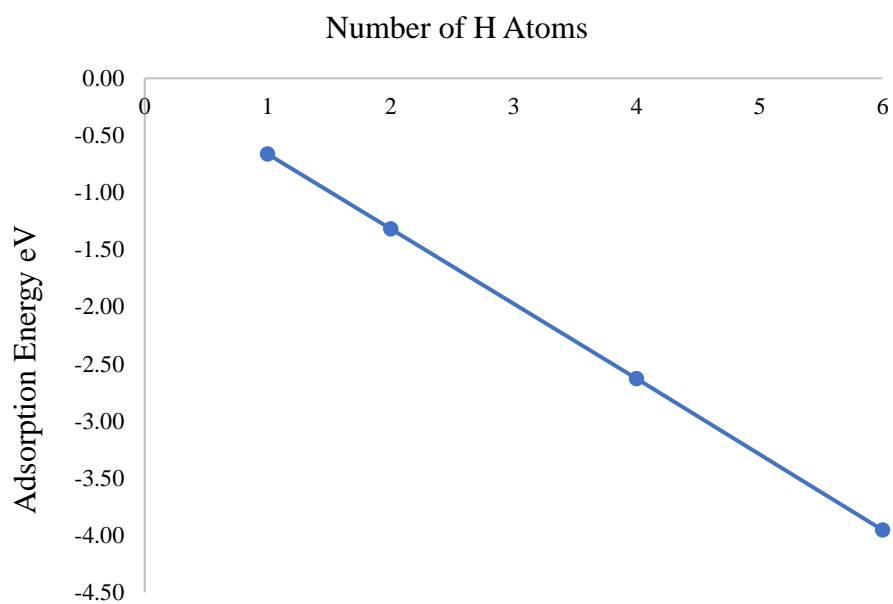


Figure 7.1: Adsorption energy (eV) correlation with number of adsorbed H atoms.

## 7.3 Other Bulk Lattice Calculations

Table 7.3: Space group and bulk unit cell energy (eV) of Ni-based IMC systems.

Unit Cell	Space Group	Bulk Energy eV
NiGa	Pm3m	-9.27
Ni <sub>3</sub> Sn	Pm3m	-22.66
NiZn	P4/mmm	-8.01
Ni <sub>3</sub> Sn <sub>4</sub>	C2/m	-71.28

Table 7.4: Bulk lattice parameters calculated using DFT-D3 and compared to experimental values. The two numbers in NiZn and Ni<sub>3</sub>Sn<sub>4</sub> lattice correspond to a and c, respectively.

	Calculated	Experimental	Error%
NiGa	2.92	2.88	1.25
Ni <sub>3</sub> Sn	3.68	3.74	1.44
NiZn	2.75	2.67	2.82
	3.18	3.24	1.87
Ni <sub>3</sub> Sn <sub>4</sub>	12.20	11.74	3.78
	5.22	5.20	0.33

## BIBLIOGRAPHY

1. Bos ANR, Westerterp KR. Mechanism and kinetics of the selective hydrogenation of ethyne and ethene. *Chemical Engineering and Processing: Process Intensification*. 1993 Feb;32(1):1–7.
2. Takht Ravanchi M, Sahebdehfar S, Komeili S. Acetylene selective hydrogenation: a technical review on catalytic aspects. *Reviews in Chemical Engineering*. 2017;34(2):215–37.
3. Urmès C, Schweitzer JM, Cabiac A, Schuurman Y. Kinetic study of the selective hydrogenation of acetylene over supported palladium under tail-end conditions. *Catalysts*. 2019;9(2).
4. Chen Y, Chen J. Selective hydrogenation of acetylene on SiO<sub>2</sub> supported Ni-In bimetallic catalysts: Promotional effect of In. *Applied Surface Science*. 2016;387:16–27.
5. Vignola E, Steinmann SN, Al Farra A, Vandegehuchte BD, Curulla D, Sautet P. Evaluating the Risk of C-C Bond Formation during Selective Hydrogenation of Acetylene on Palladium. *ACS Catalysis*. 2018;8(3):1662–71.
6. Spanjers CS, Held JT, Jones MJ, Stanley DD, Sim RS, Janik MJ, et al. Zinc inclusion to heterogeneous nickel catalysts reduces oligomerization during the semi-hydrogenation of acetylene. *Journal of Catalysis*. 2014;316:164–73.
7. Verbeek H, Sachtler WMH. The study of the alloys of platinum and tin by chemisorption. *Journal of Catalysis*. 1976;42(2):257–67.
8. Furukawa S, Komatsu T. Intermetallic Compounds: Promising Inorganic Materials for Well-Structured and Electronically Modified Reaction Environments for Efficient Catalysis. *ACS Catalysis*. 2017;7(1):735–65.
9. Osswald J, Kovnir K, Armbrüster M, Giedigkeit R, Jentoft RE, Wild U, et al. Palladium-gallium intermetallic compounds for the selective hydrogenation of acetylene. Part II: Surface characterization and catalytic performance. *Journal of Catalysis*. 2008;258(1):219–27.
10. Song Y, Laursen S. Control of surface reactivity towards unsaturated C–C bonds and H over Ni-based intermetallic compounds in semi-hydrogenation of acetylene. *Journal of Catalysis*. 2019;372:151–62.
11. Rao DM, Zhang ST, Li CM, Chen Y Di, Pu M, Yan H, et al. The reaction mechanism and selectivity of acetylene hydrogenation over Ni-Ga intermetallic compound catalysts: A density functional theory study. *Dalton Transactions*. 2018;47(12):4198–208.
12. Xu L, Stangland EE, Mavrikakis M. Ethylene versus ethane: A DFT-based selectivity

- descriptor for efficient catalyst screening. *Journal of Catalysis*. 2018;362:18–24.
13. Cao Y, Sui Z, Zhu Y, Zhou X, Chen D. Selective Hydrogenation of Acetylene over Pd-In/Al<sub>2</sub>O<sub>3</sub> Catalyst: Promotional Effect of Indium and Composition-Dependent Performance. *ACS Catalysis*. 2017;7(11):7835–46.
  14. Kim WJ, Shin EW, Kang JH, Moon SH. Performance of Si-modified Pd catalyst in acetylene hydrogenation: Catalyst deactivation behavior. *Applied Catalysis A: General*. 2003;251(2):305–13.
  15. Kim WJ, Moon SH. Modified Pd catalysts for the selective hydrogenation of acetylene. *Catalysis Today*. 2012;185(1):2–16.
  16. Armbrüster M. Intermetallic compounds in catalysis—a versatile class of materials meets interesting challenges. *Science and Technology of Advanced Materials*. 2020;21(1):303–22.
  17. Rößner L, Armbrüster M. Electrochemical Energy Conversion on Intermetallic Compounds: A Review. *ACS Catalysis*. 2019;9(3):2018–62.
  18. Dasgupta A, Rioux RM. Intermetallics in catalysis: An exciting subset of multimetallic catalysts. *Catalysis Today*. 2019;330:2–15.
  19. Yang T, Feng Y, Ma R, Li Q, Yan H, Liu Y, et al. Improvement of Selectivity in Acetylene Hydrogenation with Comparable Activity over Ordered PdCu Catalysts Induced by Post-treatment. *ACS Applied Materials and Interfaces*. 2021;13(1):706–16.
  20. Vignola E, Steinmann SN, Le Mapihan K, Vandegheuchte BD, Curulla D, Sautet P. Acetylene Adsorption on Pd-Ag Alloys: Evidence for Limited Island Formation and Strong Reverse Segregation from Monte Carlo Simulations. *Journal of Physical Chemistry C*. 2018;122(27):15456–63.
  21. Chen X, Li M, Guan J, Wang X, Williams CT, Liang C. Nickel-silicon intermetallics with enhanced selectivity in hydrogenation reactions of cinnamaldehyde and phenylacetylene. *Industrial and Engineering Chemistry Research*. 2012;51(9):3604–11.
  22. Cao Y, Zhang H, Ji S, Sui Z, Jiang Z, Wang D, et al. Adsorption Site Regulation to Guide Atomic Design of Ni–Ga Catalysts for Acetylene Semi-Hydrogenation. *Angewandte Chemie*. 2020;132(28):11647–52.
  23. Rao DM, Sun T, Yang Y Sen, Yin P, Pu M, Yan H, et al. Theoretical study on the reaction mechanism and selectivity of acetylene semi-hydrogenation on Ni-Sn intermetallic catalysts. *Physical Chemistry Chemical Physics*. 2019;21(3):1384–92.
  24. Studt F, Abild-Pedersen F, Bligaard T, Sørensen RZ, Christensen CH, Nørskov JK. Identification of non-precious metal alloy catalysts for selective hydrogenation of acetylene. *Science*. 2008;320(5881):1320–2.

25. Li C, Chen Y, Zhang S, Xu S, Zhou J, Wang F, et al. Ni-In intermetallic nanocrystals as efficient catalysts toward unsaturated aldehydes hydrogenation. *Chemistry of Materials*. 2013;25(19):3888–96.
26. Okamoto H, Schlesinger ME, Mueller EM. In (Indium) Binary Alloy Phase Diagrams. In: *Alloy Phase Diagrams*. ASM International; 2016. p. 429–46.
27. Okamoto H, Schlesinger ME, Mueller EM. Ni (Nickel) Binary Alloy Phase Diagrams. In: *Alloy Phase Diagrams*. ASM International; 2016. p. 520–33.
28. Kresse G, Furthmuller J. Efficiency of ab-initio total energy calculations for metals and semiconductors using a plane-wave basis set. *Computational Materials Science*. 1996 Jul;6(1):15–50.
29. Kresse G. Efficient iterative schemes for ab initio total-energy calculations using a plane-wave basis set. *Physical Review B*. 1996 Oct;54(16):11169–86.
30. Kresse G, Joubert D. From ultrasoft pseudopotentials to the projector augmented-wave method. *Physical Review B*. 1999 Jan;59(3):1758–75.
31. Blochl PE. augmented-wave. *PHYSICAL REVIEW B*. 1994;50:17953–79.
32. Perdew JP, Burke K, Ernzerhof M. Generalized gradient approximation made simple. *Physical Review Letters*. 1996 Oct 28;77(18):3865–8.
33. Grimme S, Antony J, Ehrlich S, Krieg H. A consistent and accurate ab initio parametrization of density functional dispersion correction (DFT-D) for the 94 elements H-Pu. *J Chem Phys*. 2010;132:154104.
34. Grimme S, Ehrlich S, Goerigk L. Effect of the damping function in dispersion corrected density functional theory. *Journal of Computational Chemistry*. 2011 May;32(7):1456–65.
35. Monkhorst HJ, Pack JD. Special points for Brillouin-zone integrations\*. Vol. 13, NUMBER. 1976.
36. Henkelman G, Uberuaga BP, Jónsson H. Climbing image nudged elastic band method for finding saddle points and minimum energy paths. *Journal of Chemical Physics*. 2000;113(22):9901–4.
37. Henkelman G, Jónsson H. A dimer method for finding saddle points on high dimensional potential surfaces using only first derivatives. *Journal of Chemical Physics*. 1999;111(15):7010–22.
38. Jain A, Ong SP, Hautier G, Chen W, Richards WD, Dacek S, et al. Commentary: The materials project: A materials genome approach to accelerating materials innovation. Vol. 1, *APL Materials*. 2013. p. 11002.
39. Goerigk L. A Comprehensive Overview of the DFT-D3 London-Dispersion Correction. 1st



- ed. *Non-Covalent Interactions in Quantum Chemistry and Physics: Theory and Applications*. Elsevier Inc.; 2017. 195–219 p.
40. Beck, U.; Neumann, H.G.; Becherer G. Phasenbildung in Ni/Si-Schichten. *Kristall und Technik*. 1973;8:1125–9.
  41. Hellner E. Das System Nickel-Indium. *Zeitschrift fuer Metallkunde*. 1950;41:401–6.
  42. Yang H, Whitten JL. Dissociative adsorption of H<sub>2</sub> on Ni(111). *The Journal of Chemical Physics*. 1993;98(6):5039–49.
  43. López N, Vargas-Fuentes C. Promoters in the hydrogenation of alkynes in mixtures: Insights from density functional theory. *Chemical Communications*. 2012;48(10):1379–91.
  44. Osswald J, Giedigkeit R, Jentoft RE, Armbrüster M, Girgsdies F, Kovnir K, et al. Palladium-gallium intermetallic compounds for the selective hydrogenation of acetylene. Part I: Preparation and structural investigation under reaction conditions. *Journal of Catalysis*. 2008;258(1):210–8.